Ocean Circulation Kinetic Energy: Reservoirs, Sources, and Sinks

Raffaele Ferrari and Carl Wunsch

Department of Earth, Atmospheric and Planetary Sciences, Massachusetts Institute of Technology, Cambridge, Massachusetts 02139; email: raffaele@mit.edu

Annu. Rev. Fluid Mech. 2009. 41:253–82

First published online as a Review in Advance on August 18, 2008

The *Annual Review of Fluid Mechanics* is online at fluid.annualreviews.org

This article's doi:
10.1146/annurev.fluid.40.111406.102139

0066-4189/09/0115-0253$20.00

Key Words

energy spectrum, geostrophic eddies, internal waves, turbulent cascade

Abstract

The ocean circulation is a cause and consequence of fluid scale interactions ranging from millimeters to more than 10,000 km. Although the wind field produces a large energy input to the ocean, all but approximately 10% appears to be dissipated within about 100 m of the sea surface, rendering observations of the energy divergence necessary to maintain the full water-column flow difficult. Attention thus shifts to the physically different kinetic energy (KE) reservoirs of the circulation and their maintenance, dissipation, and possible influence on the very small scales representing irreversible molecular mixing. Oceanic KE is dominated by the geostrophic eddy field, and depending on the vertical structure (barotropic versus low-mode baroclinic), direct and inverse energy cascades are possible. The pathways toward dissipation of the dominant geostrophic eddy KE depend crucially on the direction of the cascade but are difficult to quantify because of serious observational difficulties for wavelengths shorter than approximately 100–200 km. At high frequencies, KE is dominated by internal waves with near-inertial frequencies (frequencies near the local Coriolis parameter), whose shears appear to be a major source of wave breaking and mixing in the ocean interior.

1. INTRODUCTION

That turbulent mixing processes in the ocean are extremely important in determining the oceanic general circulation, and are major limiting factors in the ability to calculate future climate states, is a cliché in oceanography and climate dynamics. Unlike some other hackneyed statements, this one does retain much of its validity. The examination of various attempts at the prediction of ocean changes under global atmospheric warming (or any other climate hypothesis) makes apparent the presence of many sources of error. Predictions running from decades to thousands of years must be regarded as being physically conceivable scenarios and not as true forecasts (in the weather sense). A number of sources provide some idea of the divergence of models under nominally fixed conditions and of the limited understanding of their known biases (e.g., Houghton et al. 2001, IPCC 2007, Large & Danabasoglu 2006). Much, but definitely not all, of that divergence is readily attributed to differing inferences about how the ocean mixes and, consequently, great uncertainty about how those processes would change under modified climate conditions.

The tight relationship between the large-scale circulation and small-scale mixing is a consequence of the turbulent nature of oceanic flows, with energy continuously exchanged among all scales of motion. Large-scale structures cannot be analyzed in isolation from smaller-scale swirls and billows. The study of the turbulent mixing of tracers in the ocean goes back many decades and begins with the representation of very-large-scale temperature and salinity distributions, written generically as $C(\mathbf{r}, t)$, in terms of the turbulent diffusion governed by eddy coefficients in forms such as

$$\mathbf{v} \cdot \nabla C = \nabla \cdot (\mathbf{K} \nabla C), \tag{1}$$

with $\mathbf{v}$ the three-dimensional (3D) velocity field and $\mathbf{K}$ a mixing tensor. It is only comparatively recently that major attention shifted from attempts to simply determine $\mathbf{K}$ from observed large-scale distributions of property C through various forms of inverse calculation (e.g., Hogg 1987) toward understanding the fundamental turbulence giving rise to $\mathbf{K}$.

We recently reviewed knowledge of the origin of the turbulence, and the power requirements necessary to sustain it (Wunsch & Ferrari 2004). Thorpe (2005) conveniently covers much of the wider background. A number of interesting and important developments in the interim lead us to partially update the earlier review, focusing particularly on the kinetic energy (KE) budget of the ocean. Total oceanic energy necessarily includes the internal energy and potential energy (PE) as well, but the kinetic component is most directly related to the displacement of fluid parcels and hence the provision of the shear necessary to bring about irreversible mixing at molecular scales.[1] A loose emphasis on the KE also permits us to limit the scope of this review, at the same time justifying ranging across a wide variety of oceanographic phenomena without making any claim to being comprehensive.

It is convenient to work in a framework of a qualitative separation of oceanic motions—KE—by frequency band. To this end, **Figures 1** and **2** present power density spectral estimates of horizontal KE from a few reasonably representative locations in the deep open ocean; location maps are in **Figure 3**. Various databases contain over 2000 such records, and an exhaustive study of the archives is not intended. Qualitatively, however, there are some nearly universal features of such records that are useful for organizing a discussion.

All the spectral density estimates display a low-frequency, nearly white (flat) band at periods longer than approximately 1000 h (40 days). This band then falls in an approximate power law σ^{-q}

[1]Irreversible mixing happens only at molecular scales at which KE is converted into disorganized molecular agitation. Turbulent stirring can twist and fold tracer and momentum into convoluted patches, but it cannot irreversibly mix them. In this review, we use the term mixing to refer to molecular mixing, whereas we use the term turbulent mixing to describe the stirring and folding.

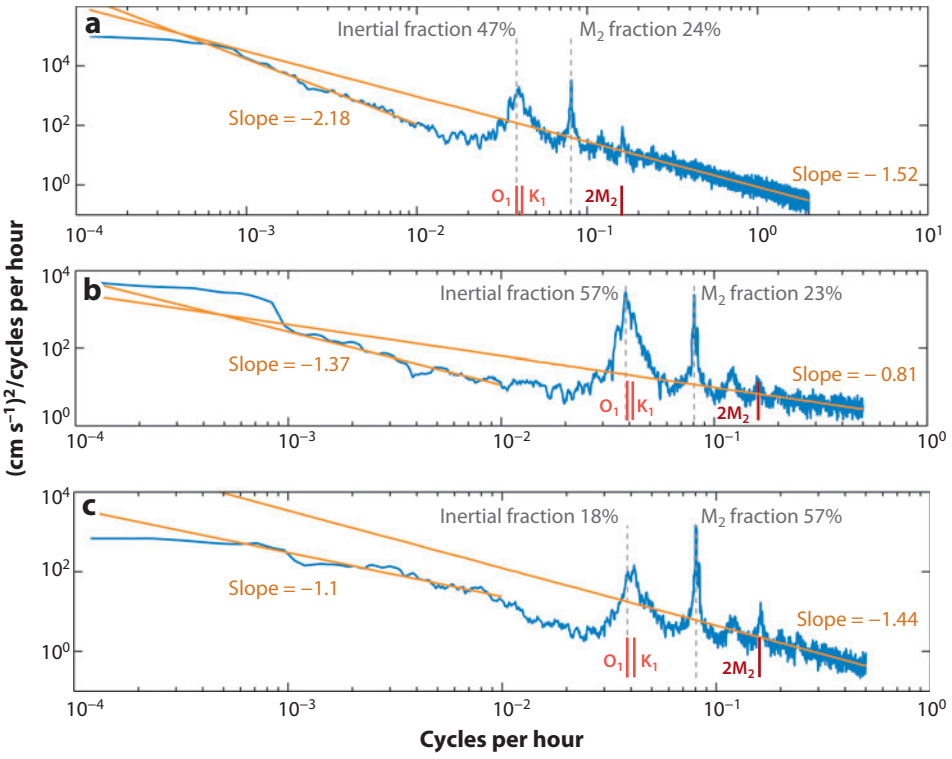

Figure 1

Kinetic energy spectral estimates for instruments on a mooring over the Mid-Atlantic Ridge near 27°N (Fu et al. 1982). The inertial, principal lunar semidiurnal M_2, and diurnal O_1, K_1 tidal peaks are marked, along with the percentage of kinetic energy in them and the kinetic energy lying between f and the highest frequency estimate. Least-squares power-law fits for periods between 10 and 2 h and for periods lying between 100 and 1000 h are shown. The approximate percentage of energy of the internal wave band lying in the inertial peak and the M_2 peak is noted. In most records, the peak centered near f is broader and higher than the one appearing at the M_2 frequency. When f is close to the diurnal frequency, it is also close to one-half the frequency of M_2, when the parametric subharmonic instability can operate. Some spectra show the first overtone, 2 M_2 of the semidiurnal tide. Instrument at (*a*) 128 m, (*b*) 1500 m, and (*c*) 3900 m (near the bottom). The geostrophic eddy band is greatly reduced in energy near the bottom, as is the inertial band, presumably because of the proximity of steep topography. Note the differing axis scales.

(where σ is the radian frequency, and q is an empirical constant), which we call the geostrophic eddy range. A conspicuous inertial peak exists at $\sigma \approx f$, where $f = 2\Omega \sin\theta$ is the Coriolis frequency equal to twice Earth's rotation period Ω multiplied by the sine of the latitude, θ, and separates the geostrophic eddy band from higher-frequency nongeostrophic motions.[2] At frequencies $\sigma > f$, there is another approximate power-law band usually identified as internal waves. A number of other features, especially tidal lines, appear in most of the records (discussed below). In all

[2]In this review, as in the oceanographic literature, the term inertial waves refers to those waves in a stratified rotating fluid with radian frequency $\sigma \approx f$. They should be distinguished from the alternative use in rotating nonstratified fluids as waves with $0 \leq \sigma \leq f$ (e.g., Chandrasekhar 1968). Here internal waves denote those motions $f \leq \sigma \leq N$, which include inertial waves as a special case. Analogous motions exist in fluids for which $N \leq \sigma \leq f$, including $N = 0$, but such conditions are almost nonexistent in the ocean.

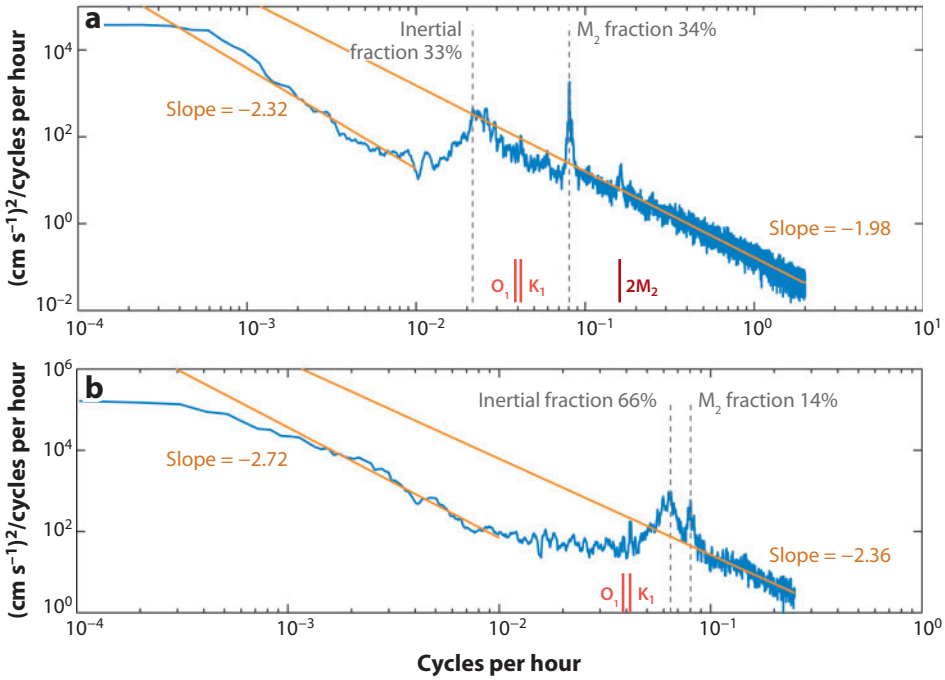

Figure 2

(*a*) Kinetic energy estimate for an instrument in the western North Atlantic near 15°N at 500 m. In this record, the diurnal tides are well separated from the inertial frequency. This record was described by Fu et al. (1982). (*b*) Power density spectral estimate from a record at 1000 m at 50.7°S, 143°W, south of Tasmania in the Southern Ocean (Phillips & Rintoul 2000). Now the diurnal tides are below f in frequency, but whether the apparent peaks represent dominantly barotropic or baroclinic motions is not known.

cases, there is a sample time average velocity $\bar{u}$, $\bar{v}$, with a KE, $1/2(\bar{u}^2 + \bar{v}^2)$, that is commonly indistinguishable from zero in open ocean records.

Frequencies $\sigma < f$ are thought to be almost completely geostrophically balanced at least below the surface boundary layers,[3] whereas those $f < \sigma < N$ are controlled by gravity wave dynamics. The transitional inertial peak is dominated by gravity wave physics strongly modified by rotation, and with important effects from the latitudinal variation, $\beta = R^{-1} df/d\theta$, where R is Earth's radius. Frequencies $\sigma > N$ are thought to be primarily small-scale turbulent motions resulting from breaking of the lower-frequency internal waves.

Much fluid physics is known not in the context of frequency, but rather in the context of wave-number spectra. Only a few wave-number spectral estimates of ocean variability exist (e.g., Katz 1975, Stammer 1997) and tend, qualitatively, to be red (i.e., with energy generally increasing with wavelength) without the distinctive features seen in the frequency domain. Theory suggests a major overlap in the wave-number domain of the different timescales seen in the displayed frequency spectra. Frequency-wave-number spectra are required to delineate space scales, and thus much theoretical discussion (see below) of energy transfers in wave-number cascades tends to be highly speculative because measurements capable of producing frequency-wave-number separation are

[3]Geostrophy results from near-exact balance between the Coriolis force and the pressure gradient force. At the ocean surface (at which air-sea fluxes are strong and velocities large), frequencies $\sigma < f$ are still nearly balanced, but the condition involves more forces.

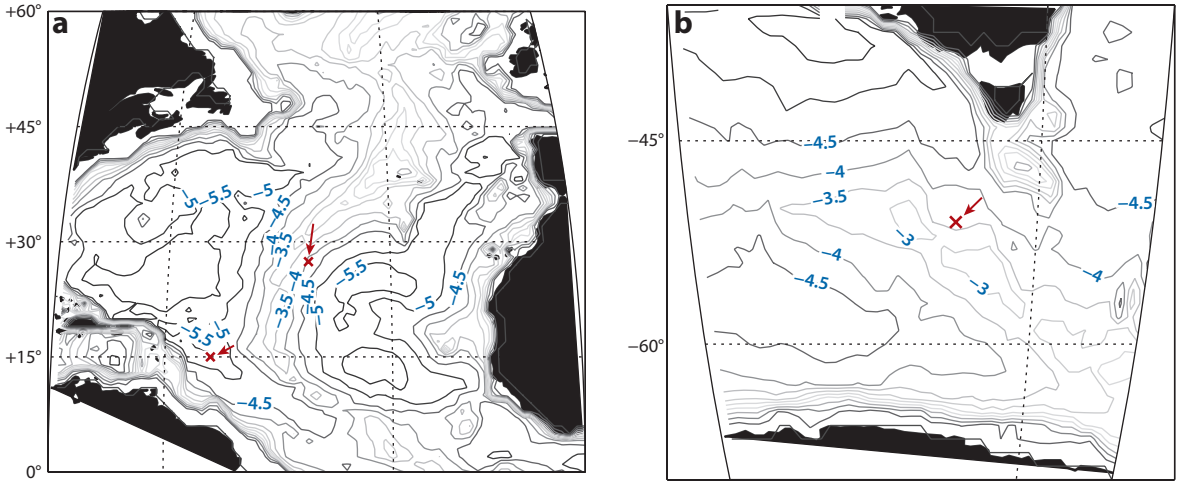

Figure 3

(*a*) Location chart for the North Atlantic current meter records used in this review. One mooring lies in the complicated 3D topography of the Mid-Atlantic Ridge, whereas the other lies over an abyssal plain. (*b*) Position of the Southern Ocean current meter whose kinetic energy spectral estimate is displayed in Figure 2*b* (Phillips & Rintoul 2000). Depths are in kilometers for both panels.

expensive and rarely available. The few estimates that exist (see Munk 1981, Zang & Wunsch 2001) require assumptions about separability, have restricted ranges, and are geographically highly localized. A recurring theme here is the essential need for frequency-wave-number separation capabilities in oceanography, particularly at length scales shorter than approximately 200 km, at which several distinct physical processes are present.

Supplemental Figure 2 presents a schematic of the frequency-wave-number spectrum (follow the **Supplemental Material** link from the Annual Reviews home page at **http://www.annualreviews.org**). How are these spectra maintained? Where does the energy come from? Is it redistributed in frequency and/or wave-number space? How is it dissipated, and how much of the dissipated energy contributes to oceanic mixing processes? Are the seemingly different dynamical ranges coupled?

2. THE OCEANIC ENERGY BUDGET

We begin this section by briefly recapitulating and updating the discussion of the total energy budget of the ocean. Wunsch & Ferrari (2004) attempted an order-of-magnitude estimate of the major reservoirs and energy transfers toward dissipation in the global ocean (for a modified and updated version, see **Supplemental Figure 1**). Many of the numbers remain highly uncertain, and some are missing entirely. It is characteristic of the ocean circulation that important energy reservoirs differ by orders of magnitude in the amount of energy resident in each. To a great extent, the size of the reservoirs is irrelevant; the amount of energy (a few tens of exajoules per year) required to sustain the oceanic general circulation is so slight compared to the magnitude of the energy reservoirs that determining the pathways of flow through the system is difficult.

The geostrophic eddy field[4] dominates the energy content at subinertial frequencies, whereas mixed layer turbulence is the largest reservoir at superinertial frequencies. The overlap in

[4]Geostrophic eddies are commonly called mesoscale eddies, which is a misnomer (in the atmospheric literature, they are referred to as synoptic scale eddies), but we sometimes use the terminology.

wave-number space (**Supplemental Figure 2**) is difficult to observe and proves an important obstacle to understanding the behavior of the circulation.

The stress applied by the atmospheric winds at the ocean surface provides the energy to keep the oceanic KE spectrum in equilibrium in the upper ocean. The situation is less clear in the abyssal ocean. Munk & Wunsch (1998) estimated that approximately 2 TW of power is required to maintain the abyssal KE spectrum by using the observed deep stratification and an assumption of how much bottom water had to be returned vertically to approximately 1500 m. Whitehead & Wang (2008) produced a laboratory demonstration of this balance in a salinity stratified fluid, in which the rate of upwelling of abyssal waters was linearly proportional to the energy expended in turbulent mixing of the fluid.

Hughes & Griffiths (2006) claimed that much of the bottom water is entrained at great depths and only a fraction of the fluid is returned to 1500 m so that the power required might be as little as 0.2 TW. Some reduction from 2 TW seems reasonable, but North Atlantic Deep Water, for example, appears to be fully formed by 1000 m depth, with little or no entrainment below. St. Laurent & Simmons (2006) made an independent estimate by calculating the power requirement to sustain the observed (inferred) turbulent mixing in the ocean interior from a great variety of methods and places. Their summary total is that approximately 3 ± 1 TW are required for the whole water column. Possibly important upper ocean dissipation regions are ignored (e.g., convective regions, continental margins). Of their total, somewhere between one-third and one-half of the total power would be required above ~1500 m, thus requiring approximately 1.5–2 TW for the abyssal ocean. Estimates of oceanic mixing, mixing efficiencies, and the power required warrant full reviews of their own.

Toggweiler & Samuels (1995) speculated that some fraction of North Atlantic Deep Water is pulled toward the surface by the strong winds blowing along the Antarctic Circumpolar Current: The winds drive a divergent Ekman flow that results in upwelling of subsurface waters. This plausible scenario has support from some observations (Speer et al. 2000) and suggests that a possibly large fraction of the power necessary to close the overturning circulation of the ocean is supplied by surface winds.

2.1. Upper Ocean/Lower Ocean

One difficulty with global energy budgets is that they lump regional processes that may be markedly different from the volume average into crude global integrals. In the context of the global energy budget, the upper ocean clearly behaves qualitatively differently from the abyssal one. As early as Defant (1961), the ocean was divided into a "troposphere" and "stratosphere," and it was clear that the dynamics of the (roughly) upper 1000 m of the ocean had to be quite different from that below. The separation between upper and abyssal oceans is deliberately a bit vague here, but, depending on position, lies somewhere between 1000 and 2000 m in depth. The separation is more pronounced at low and mid-latitudes, whereas it is blurred in polar regions in which deep convective events can mix the whole water column. The surface mixed layer represents a third region requiring separate treatment.

Wunsch & Ferrari (2004) derive the KE budget for the global ocean with the KE per unit mass defined as $E = 1/2\mathbf{u} \cdot \mathbf{u}$. In steady state, E is constant, and

$$\iint [p\mathbf{u} + \rho\nu\nabla E] \cdot \hat{\mathbf{n}} \mathrm{d}A = -\iiint g\rho w \mathrm{d}V + \iiint p\nabla \cdot \mathbf{u} \mathrm{d}V - \iiint \rho\varepsilon \mathrm{d}V, \qquad (2)$$

where p is the pressure, ρ is the density of seawater, ν is the kinematic viscosity, V is the total volume of the ocean, A is the surface of that volume, and $\hat{\mathbf{n}}$ is the unit outward normal. In deriving

Equation 2, trivial air-sea momentum exchanges due to evaporation and precipitation are neglected. Surface forcing comprises the work done by differential pressure and viscous stresses acting on the moving free surface. The three terms on the right-hand side represent the conversion of KE into PE, into compressive internal energy and viscous dissipation. The viscous dissipation ε is the irreversible conversion of KE into heat, and for nearly incompressible fluids such as seawater, it takes the form

$$\varepsilon = \frac{1}{2}\nu \sum_{i=1}^{3}\sum_{j=1}^{3}\left(\frac{\partial u_i}{\partial x_j} + \frac{\partial u_j}{\partial x_i}\right)^2, \tag{3}$$

where $(x_1, x_2, x_3) = (x, y, z)$ and $(u_1, u_2, u_3) = (u, v, w)$.

Wunsch & Ferrari (2004) show that generation and destruction of the oceanic potential and internal energy are confined to the surface mixed layer because the vertical fluxes of heat and freshwater vanish when integrated on a level surface in the ocean interior. At equilibrium, the KE generated by surface stresses and forces is balanced by viscous dissipation—a contrast to the atmospheric situation in which solar heating is absorbed and radiated throughout, resulting in interior sources and sinks of potential and internal energy. The vanishing of the conversions to potential and compressive internal energies is not trivial because it is the result of several much larger conversion terms. Wunsch & Ferrari (2004) show that the integral on a level surface of these two terms is equal to the integral of the conversion term, $g\rho_\theta w$, representing the net KE required to lift a water parcel, once reversible adiabatic effects have been subtracted (ρ_θ is potential density, i.e., the density of a water parcel brought to the ocean surface to eliminate compressive effects),

$$\iint g\rho_\theta w \,\mathrm{d}S \approx \iint g\rho w \,\mathrm{d}S \approx -\iint p\nabla\cdot\boldsymbol{u}\mathrm{d}S.$$

The two variables (ρ_θ, w) contributing to the $g\rho_\theta w$ conversion term can be decomposed into three components owing to mean motions and subinertial and superinertial fluctuations,

$$(\rho_\theta, w) = (\bar{\rho}_\theta, \bar{w}) + (\rho'_{\theta g}, w'_g) + (\rho'_{\theta t}, w'_t), \tag{4}$$

where the subscripts are a reminder that subinertial fluctuations are typically geostrophic and superinertial ones include internal waves and small-scale turbulence. Because the gravitational and compressive works vanish when integrated on a level surface, the integral of $g\rho_\theta w$ at any level in the ocean interior must also vanish,

$$\iint g\rho_\theta w \,\mathrm{d}S \approx \iint g\bar{\rho}_\theta \bar{w}\mathrm{d}S + \iint g\overline{\rho'_{\theta g} w'_g}\,\mathrm{d}S + \iint g\overline{\rho'_{\theta t} w'_t}\,\mathrm{d}S \approx 0. \tag{5}$$

Geostrophic fluctuations represent a release of large-scale PE through subinertial instabilities, without any irreversible mixing, and can be thought of as advection by a generalized Stokes drift $\bar{w}^{\uparrow}$ (Plumb & Ferrari 2005), i.e., $\overline{\rho'_{\theta g} w'_g} \approx g\bar{\rho}_\theta \bar{w}^{\uparrow}$. Superinertial turbulent fluctuations are the pathway to irreversible mixing through small-scale instabilities.

Theories of the upper ocean, not ruled out by observation, suggest that turbulent fluctuations leading to irreversible mixing are confined to the surface mixed layer but are negligible in the interior; that is, the circulation is nearly adiabatic in character (e.g., Pedlosky 1996, Vallis 2006, Webb & Suginohara 2001). The balance in Equation 5 is therefore between the first two terms. The mean contribution represents the transfer from KE to PE that occurs when the wind-driven Ekman flux raises the ocean's center of gravity by pushing down light fluid in the subtropical regions and pulling up dense fluid in the subpolar regions. The subinertial contribution is through the release of PE by baroclinic instabilities (i.e., the slumping of lateral density gradients).

In the abyss, the sum of the mean and subinertial eddy contributions balances the generation of PE by turbulent mixing through internal wave breaking. Mean and subinertial components oppose each other as in the upper ocean, but they do not compensate for each other to the same degree. Hence the energy expended by turbulent mixing supports the upwelling of buoyancy by the sum of the Eulerian mean and the generalized Stokes drift velocities (i.e., by the generalized Lagrangian mean velocity). Many authors seem to have confused the Eulerian and Lagrangian mean velocities in this budget.

3. EXTERNAL SOURCES OF KINETIC ENERGY

External forces acting to set the ocean into motion on any scale are restricted in number, and overall there is not a great deal of new insight available since Wunsch & Ferrari (2004) (for an update of the literature, see the **Supplemental Appendix**).

The wind field is by far the dominant energy source to the ocean and can be regarded, oceanographically, simply as a reservoir of atmospheric KE directly transferable into the ocean. The coupling of the generation of different energy forms in the dynamics (in either balanced or wave motions) means one cannot generate or dissipate KE without also generating (dissipating) PE. Thus wind work on the ocean can be regarded either as directly producing KE (e.g., the large-scale ocean circulation) or instead producing its PE through the $g\bar{\rho}_\theta \bar{w}$ conversion term [as in Gill et al.'s (1974) picture of Ekman pumping/suction working against the mean stratification], and the conversion of atmospheric KE cannot be regarded as going solely into one type of oceanic energy.

The sum of the two terms on the left-hand side of the KE budget in Equation 2 represents the total working rate of the wind on the sea surface. Wang & Huang (2004) have calculated these terms, paying specific attention to the generation of the wave field, and conclude that the net value is close to 60 TW. Csanady (2001) shows that the terms on the right-hand side of Equation 2 are typically an order of magnitude larger in the near-surface ocean than in the interior: The oceanic energy budget is closed to better than 10% in the surface mixed layer alone. The interior circulation is driven by the small residual of energy that fluxes through the mixed layer base, making quantitative calculations and observations difficult.

3.1. Stress Acting on the Geostrophic Circulation

Let us consider first the work done on the geostrophic circulation. At the scales of geostrophic motions, the ocean surface is approximately horizontal, and the working rate is approximately

$$W_{wind} \approx \iint_{ocean} \rho \nu \frac{\partial}{\partial z}\left(\frac{1}{2}\mathbf{v}^2\right) dA = \iint_{ocean} \boldsymbol{\tau} \cdot \mathbf{v}_g dA, \tag{6}$$

where $\mathbf{v}_g$ is the surface geostrophic flow in the ocean (the equatorial band, 1–2° of latitude on either side of the equator, requires special treatment). The wind stress acting on the ocean has typically been computed from the turbulent drag formula

$$\boldsymbol{\tau}_1 = C_D \rho_{air} |\mathbf{v}_a| \mathbf{v}_a, \tag{7}$$

where C_D is an empirical coefficient dependent on air-sea temperature differences and the wind speed itself, ρ_{air} is the air density, and $\mathbf{v}_a$ is the vector atmospheric wind, usually at 10-m elevation. Wunsch (1998) estimated a net work rate of 0.8 TW with approximately 80% entering in the Southern Ocean. Von Storch et al. (2007) recalculated the rate of work done on the subinertial circulation (i.e., they substituted the full subinertial surface velocity for $\mathbf{v}_g$) using a much higher-resolution model and estimated a net work rate of 3.8 TW on the upper ocean, but only 1.1 TW

was associated with work done on the geostrophic velocity and reached the ocean beneath the very surface layer. All the power input to the surface Ekman layer was dissipated there.

These and similar calculations likely have significant positive biases: Dewar & Flierl (1987), Cornillon & Park (2001), Chelton et al. (2004), Dawe & Thompson (2006), Duhaut & Straub (2006), Zhai & Greatbatch (2007), and Hughes & Wilson (2008) demonstrate that $\boldsymbol{\tau}$ in Equation 7 is significantly inaccurate—because it must depend on the water velocity, $\mathbf{v}_o$, relative to the air, probably in the form

$$\boldsymbol{\tau}_2 = C_D \rho_{air} |\mathbf{v}_a - \mathbf{v}_o| (\mathbf{v}_a - \mathbf{v}_o). \tag{8}$$

Wind velocities are so much higher than water velocities, and the spatial structure of the wind field is so much larger than that in the ocean that $\boldsymbol{\tau}_2$ is conventionally approximated by $\boldsymbol{\tau}_1$. The interesting difficulty is that the modification to the stress by small-scale oceanic motions is a negative-definite systematic correction. When $|\mathbf{v}_o| \ll |\mathbf{v}_a|$,

$$\boldsymbol{\tau}_2 \cdot \mathbf{v}_o = \boldsymbol{\tau}_1 \cdot \mathbf{v}_o - C_D \rho_{air} \frac{|\mathbf{v}_a \cdot \mathbf{v}_o|^2}{|\mathbf{v}_a|} - C_D \rho_{air} \frac{|\mathbf{v}_a|^2 |\mathbf{v}_o|^2}{|\mathbf{v}_a|}. \tag{9}$$

Because of their differing space/timescales, ocean eddy perturbations are weakly correlated with the major atmospheric wind patterns, but they do contribute to the reduction in Equation 9. More than 90% of the surface KE in the ocean lies in the eddy field (Wunsch 2007, plate 6), and the reduction in Equation 9 scales as $v_{eddy}^2 / v_a v_{mean}$. Spatially smoothing ocean currents leads to an increase in the power input by the wind compared with that for an unsmoothed flow (Hughes & Wilson 2008)—that is, at high wave numbers, stress and oceanic surface flows are negatively correlated.

An analogous effect arises (Behringer et al. 1979, Dewar & Flierl 1987) from the dependence of C_D on air-sea temperature differences, which also has an eddy-scale effect, although not necessarily of one sign. The temperature sensitivity may be most important in its systematic effects in strong western boundary currents. For winds in excess of 60 m s^{-1} (Jones & Toba 2001), the drag coefficient C_D increases quadratically with wind speed. At these extreme values, the ocean surface becomes a mixture of air and water (referred to as sea spray). The two-phase mixture modifies the transfer of momentum between the atmosphere and the ocean, and conventional bulk formulas fail. No estimates exist of such effects on the oceanic energy budget, although the impact of the sea-spray regime on the energy budget of hurricanes has been examined (Emanuel 2003). The exact dependence of C_D on the velocities, air-sea temperature differences, and sea state is a disputed subject in its own right.

Chelton et al. (2004) found that some correlation develops at the eddy scale between $\mathbf{v}_o$ and $\mathbf{v}_a$ because the ocean heat anomalies associated with eddies modify the stability of the atmospheric boundary layer and hence the surface winds. These feedbacks probably contribute little to Equation 9 because they represent a minor modification of $\mathbf{v}_a$, and they can contribute both positive and negative biases. Nevertheless, a careful quantification from data is lacking to make firm conclusions.

Last, but not least, temporal and spatial averages of quadratic (atmospheric) or cubic (oceanic) variables can be markedly higher than the quadratic or cubic values of the averages, especially because the statistics of stress are significantly non-Gaussian and skewed toward poorly sampled high values (Gille 2005). (We further discuss the eddy structure of the wind work in the context of the dissipation of oceanic KE below.)

3.2. Stress-Generated Inertial Waves

Wind has long been known to excite inertial motions at the sea surface and is part of the so-called Rossby adjustment problem in which any nongeostrophically balanced motion in a rotating

system tends toward balance by radiating, among other internal waves, inertial ones. Pollard & Millard (1970) represented the upper ocean through a slab model, one that has been widely used to calculate the rate of generation of inertial waves by the wind field (D'Asaro 1985). Alford (2003), using a slab, calculated a wind power deposit into inertial waves of approximately 0.5 TW.

Deriving the slab model of the flow field from the equations of motion is dependent on a series of assumptions whose validity is obscure, and thus the true uncertainty of the rates of direct energy input into the inertial wave band is not known. Plueddemann & Farrar (2006) analyzed the effects of shear at the base of the mixed layer, which acts as a damping term but is ignored in slab models, and showed that Alford's estimates of the power input to the ocean by the generation of inertial frequencies is likely overestimated by approximately a factor of two (see also Stockwell et al. 2004; S. Elipot & S. Gille, submitted manuscript). Alford & Whitmont (2007) have produced the latest compilation of the generation of inertial waves by wind; they try to account for results such as those by Plueddemann & Farrar (2006) by doubling their estimate of the damping coefficient.

4. OCEANIC KINETIC ENERGY: THE SPECTRUM

We return now to the description of the KE spectral estimates in **Figures 1** and **2**, with the expectation that a closer analysis of the differing physics of the various frequency bands can shed light on their generation, dissipation, and inter-reservoir energy transfers.

4.1. The Overall Behavior

Figure 1 shows spectral estimates from records at 27°N, 41°W in the North Atlantic. The top two spectra are representative of many open ocean records, whereas the bottom instrument is surrounded by complex 3D topography, rendering the spectral density measurably differently shaped. In all three results, one sees a distinct peak at the frequency of the principal lunar semidiurnal tide; a second peak is marked as inertial. These measurements were made at a latitude at which the frequencies of the principal diurnal tides K_1 and O_1 nearly coincide with f, although North Atlantic diurnal tides are comparatively weak (compared both to the semidiurnal tides and their amplitudes in other oceans). At frequencies above M_2, all estimates display a near power-law behavior that has been fit by least squares to $A\sigma^{-q}$, where q is typically between approximately 1.5 and 2 in most parts of the world. This oceanic internal wave band is discussed in an immense literature, much of which can be located starting with Munk (1981) or Thorpe (2005). Superimposed on this power law, and visible in both spectra, are harmonics of the tides and of the inertial peaks. The extent to which the spectra are real and are the result of fluid wave-interaction nonlinearities, as opposed to nonlinearities in the instruments or advection by larger-scale flow, is not obvious. The deepest instrument on this mooring shows a suppressed inertial band energy—unsurprising when one recognizes that the motions would necessarily reflect from steep nearby topography—generating velocity nodes at the topography (here steep refers, crudely, to slopes significantly greater than that of the internal wave group velocity vector). That inertial motions are suppressed near topographic features has been known for a long time (e.g., Wunsch 1976), and they are missing in canyon-like features. Whether steep topographic features are inertial motion energy sources, simple adiabatic reflectors, or energy sinks through instabilities and mixing cannot be determined from isolated measurements of the energy level.

As one of a large number of variants, **Figure 2*a*** comes from the tropical abyssal plane at 15°N at approximately 500 m. Diurnal tides appear above the inertial frequency, and inertial and M_2 band energies are nearly equal. It is unknown whether the reduced energy in the inertial band relative to the M_2 band is the result of displacement of the diurnal tides, the inability of the M_2 tides

to resonantly generate inertial motions (see below), or the ambient background oceanography, meteorology, and topography.

Many spectral estimates exhibit overtones of the inertial and/or tidal bands, and sometimes their sum and difference frequencies. The equations of motion are nonlinear, and such secondary peaks are not unexpected (e.g., Niwa & Hibiya 1999), but as with the power laws, instrumental issues mean overtones need to be viewed suspiciously.

A significant drop in the spectral estimates occurs at frequencies below f. At periods longer than 50–100 days, the spectra rise again in another approximate power law in the geostrophic eddy range, until they flatten into the low-frequency white noise band. Motions in this band are not well described but are often dominated by near-zonal currents. The transition between the white noise band and the spectral roll-off determines the scale at which the motions become decorrelated. A flat spectrum at scales longer than the decorrelation times suggests that low-frequency motions in the ocean behave similar to an unpredictable white noise. Frequency spectra from Lagrangian time series have a similar shape, but the spectral slope in the geostrophic eddy range is substantially steeper. (For an up-to-date review on the current technology and observations for oceanographic Langrangian-type measurements, see LaCasce 2007.) Small-scale (10-km) features are advected by the energy-containing eddies (the spectral peak), leading to a Doppler shift into the high-frequency region of the Eulerian spectrum, but no such Doppler shift appears in the Lagrangian version. The white noise band is also evident in Lagrangian spectra, but extends to higher frequencies (periods of 10 days). A shorter decorrelation timescale in Lagrangian measurements is consistent with Corrsin's (1959) conjecture: Ocean velocities decorrelate both in space and time, but Eulerian ones experience only the temporal part because they are taken at a fixed spatial position. A Lagrangian observer, by drifting, experiences both the temporal and spatial decorrelation simultaneously and generally measures a shorter decorrelation time. Middleton (1985) summarizes theory and evidence from drifters for a shorter Lagrangian decorrelation timescale.

A flat spectrum at low frequencies has important implications for estimating the lateral stirring by eddy motions. Taylor (1921) showed that the dispersive power of a turbulent velocity field [i.e., the magnitude (eigenvalues) of the mixing tensor in Equation 1] is proportional to the Lagrangian spectrum at zero frequency. The eddy kinetic energy (EKE) spectral level at the roll-off from white noise to power law gives the energy level of zero frequency because the spectral shape remains fixed. These frequencies are also proportional to the inverse Lagrangian decorrelation time (LaCasce 2007). Hence the lateral spreading of tracers in the ocean is mostly associated with geostrophic eddies having decorrelation timescales of the order of 10 days.

The explanation for the absence of a cutoff at N, when resolved by sampling, is either that the instrument noise level is too great to show the very low energy levels in what can be regarded as a turbulent band or that small nonlinearities in the instruments produce spurious high frequencies. Detailed information of the spectral transition at N can be obtained with Lagrangian-like measurements. D'Asaro & Lien (2000) estimated Lagrangian spectra from neutrally buoyant floats over and near the sill of Knight Inlet. In the internal wave range of frequencies, $f \leq \sigma \leq N$, the energy spectra were consistent with a broad continuum of energy with a power-law behavior $A\sigma^{-2}$ except for tidal and inertial peaks. At higher frequencies, $\sigma > N$, beyond the internal wave range, the spectra rapidly transitioned to a steep spectral roll-off consistent with an inertial subrange of stratified turbulence (Moum 1996). The high-frequency field of fluctuating motions apparently can be described as a sum of internal waves, $\sigma < N$, and turbulent motions with $\sigma > N$, and little interaction.

Figures 1 and **2** show the fraction of the energy for frequencies $\sigma \geq f$ that lies in the inertial peak and in the M_2 band. The energy content in the peaks was based on a subjective visual estimate of the point at which the excess energy in the peak falls to the background continuum. Peaks near

f extend below that frequency some distance into the eddy band until they match the subinertial spectral levels (and the present definition of the internal wave energy starts at that point). In the upper ocean record, approximately 50% of the internal wave KE is inertial, and approximately 20% is in the tides. In the lower record, the ratios are nearly reversed. An analysis of 138 North Atlantic records produced approximately 50% of the internal wave band variance in the inertial peak, with approximately 20% lying in the M_2 band (C. Wortham, personal communication). No global inventory exists of the relative energies of inertial motions and tides, but the perception that the KE of the inertial band is dominant, rather than the tidal one, has some rudimentary support.

The broad energy continuum between *f* and *N* in the spectra is well described by Garrett & Munk's (1972) heuristic model (GM) and its subsequent modifications (Munk 1981). The most surprising and significant aspect of the GM spectrum is its near universality. Important deviations (e.g., larger than a factor of three) from the reference form are observed only in special places such as the Arctic Basin or submarine canyons. The spectrum, however, does not account for the great variance found in the tidal and inertial peaks. In atmospheric measurements, no conspicuous inertial peak appears, and what oceanographers regard as internal waves are instead interpreted as arising from Doppler shifting of the low-frequency energetic wind fields (the Taylor hypothesis), with little contribution from wave-like phenomena (Gage & Nastrom 1986). By contrast, the oceanographic interpretation is that advection dominates at frequencies below *f* (e.g., Hua et al. 1998), whereas at higher frequencies advection is ignored altogether. The extent to which the moored oceanic spectra are contaminated by Doppler shifting to high frequencies, and the meteorological ones by internal gravity waves, is unclear, but it seems unlikely that either extreme view can be justified (e.g., Gille 2005, Pinkel 2008).

How do these spectra relate to oceanic mixing? At frequencies below *f*, the motions are very energetic (see **Supplemental Figure 1**), but have very large vertical scale (Wunsch 1997), and hence have low shear and little direct role in driving instabilities leading to irreversible mixing. The focus then becomes the internal wave band at which vertical shears can become very large (Munk 1981) and are thought to control open ocean background mixing. We return below to the question of why KE is transported most efficiently to small scales in the inertial band.

4.2. Tides in the Internal Wave Band

Tidal peaks in the spectral estimates are conspicuous but not dominant. Tidal mixing is essentially the study of internal waves of tidal period—their generation by barotropic motions, their interaction with the background internal wave field, the coupling to topography both as a generator and dissipator, and their stability in the most general sense. We note that Toole (2007) withdraws the conclusion that there was significant tidal modulation of the Brazil Basin mixing rates—undermining one of the inferential pillars of the importance of tides. Much progress in understanding internal tide generation and consequent mixing comes from the recently concluded Hawaii Ocean Mixing Experiment (see Rudnick et al. 2003). [For a detailed understanding of the generation, breakdown, and mixing from tides, we refer the reader to June 2006 issue of the *Journal of Physical Oceanography* and Xing & Davies (2006), among others.] Klymak et al. (2006), for example, conclude that 3 ± 1.5 GW of energy is dissipated by the tides near the Hawaiian Ridge with 4–7 GW of energy unaccounted for, but apparently lost by the barotropic tide. If one seeks 2 TW to power the abyssal general circulation, and if (in round numbers) 5 GW is available at Hawaii, then 400 Hawaiis can do it all. Whether such a worldwide extrapolation is a reasonable one is unknown. Internal tidal generation at topography has been reviewed by Garrett & Kunze (2007).

The nature of the boundary layers formed on slopes by tidal and other internal wave motions has received comparatively little attention (e.g., see Nash et al. 2007 for measurements). Laboratory experiments are quite striking (e.g., Ivey et al. 2008, and references therein), but field measurements at the much higher Reynolds numbers present in the open ocean would be welcome, as would laboratory studies of the boundary layers in the presence also of strong rotation.

4.3. Inertial Waves

Despite their ubiquity, energy, and many years of study, much about the behavior of inertial waves remains obscure. Above we describe how inertial oscillations are generated by a time-varying wind stress. However, as with many wave boundary value problems of Sturm-Liouville type, direct, linear, wind generation tends to excite primarily low modes (barotropic and the first few baroclinic ones), as supported by Gill's (1984) analytical model and Zervakis & Levine's (1995) numerical one. Thus although there is a great deal of energy sometimes present in directly driven motions, little shear exists. Observations, conversely, show that there are strong inertial motions in the open sea with high-shear values. The difference in vertical structure is crucial because only waves with strong shears undergo Kelvin-Helmholtz-like instabilities, leading to 3D turbulence and irreversible mixing. Low-mode waves are stable and do not affect the ocean circulation much. Balmforth & Young (1999) and Mohelis & Llewellyn Smith (2001) show that interaction with the geostrophic field, the planetary vorticity, and topography can pump inertial energy into high shears. No quantitative estimates of these effects exist.

Understanding of the generation rates of inertial waves is greatly complicated by the propagation of energy poleward in the ambient internal wave field as depicted by Munk & Phillips (1968) and Fu (1981). Wave motions at low latitudes at frequency σ can reach a latitude at which $\sigma \approx f$, generating a wave caustic with considerable structure. Fu (1981) concluded that most of the subsurface inertial energy arose from this turning latitude. These motions then would be generated from processes producing internal waves at all frequencies—including the ambient high modes—rendering the inertial wave generation problem identical to that of understanding the origin of internal waves generally. Linear wind generation within the caustic apparently has been discussed only by D'Asaro (1989), who finds a strong increase in horizontal wave numbers relative to the linear problem in which latitude variations in f are neglected.

Garrett (2001) noted that the spectral density in the frequency range $f \leq \sigma \leq 2f$ could acquire energy from internal waves above this band through the parametric subharmonic instability, and the power law at high frequencies seen in **Figures 1** and **2** is indeed much flatter than it is in the rise into the inertial peak maximum. Hibiya et al. (2002) discussed the effects of the parametric subharmonic instability, and MacKinnon & Winters (2005) found it permits the M_2 tide to efficiently transfer energy into the inertial peak at the latitude at which $\sigma_{M_2} \approx 2f$. Some field observations (van Haren 2005) seem to support the idea, whereas others (Rainville & Pinkel 2006) are ambiguous.

The significance of inertial waves for ocean mixing is unclear. A number of studies have examined their shear profile (e.g., Leaman 1976). Open ocean shear (Kelvin-Helmholtz) instability of internal waves generally appears capable of providing the background mixing (turbulent diffusivity values near 10^{-5} m^2 s^{-1}) but not the much higher values seen near complex topography that appear to dominate ocean mixing. A considerable body of literature exists concerning the interaction of high-frequency internal waves with topography (e.g., Eriksen 1985, 1998), but little of it is applicable to motions with $\sigma \approx f$, and one must account for the meridional gradient in f (the β-effect).

As with discussions of tides in ocean mixing, there are several complementary, but overlapping, problems. The Poincaré equation that governs the inviscid limit of f-plane internal waves

permits the rapid generation of high-shear regions from low-shear disturbances when topography is encountered. Laboratory studies have focused on the dissipative and instability processes, the so-called critical slope—when the internal wave characteristic (direction of the group velocity vector) slope, $c = (\sigma^2 - f^2)^{1/2}/(N^2 - \sigma^2)^{1/2}$, is approximately equal to the bottom slope γ; can produce intense motions; and, in the laboratory at least, can produce intense mixing (e.g., Ivey et al. 2000).

On a β-plane and in related approximations (Fu 1981, Munk & Phillips 1968), the group velocity is finite as $\sigma \to f$ from above, with unclear results for topographic interaction. In observations at sea, Lai & Sanford (1986) observed hurricane-generated low-vertical-mode inertial motions emanating from sloping topography to their north in what one infers to be a reflection process for barotropic motions (see Xing & Davies 2002 for a numerical study of wind-generated inertial motions and shear over a continental margin). Kunze & Sanford (1986) interpreted intensified inertial motions near Caryn Seamount close to Bermuda in the North Atlantic as resulting from an interaction with a nearby eddy rather than from topographic interaction. The sensitivity of inertial motions both to bottom slopes and to ambient fluid vorticity perturbations to f renders delicate the problem of understanding their life cycle. Young & Ben Jelloul (1997), Klein et al. (2004), and Zhai et al. (2007) show that anticyclonic geostrophic eddies focus near-inertial motions. In general circulation models, this effect leads to a spatially heterogeneous vertical mixing strongly related to the eddy-field properties, but little appears known of the realism of inertial/internal waves in these models. Xing & Davies (2002) used 60 vertical levels and a horizontal grid with 0.6-km spacing (roughly 0.005° resolution) to capture the important nonlinearities of the internal wave band. Hibiya et al. (1996) employed a resolution of 10 m horizontally and 1.25 m vertically. Such resolutions are far beyond the capability of any existing ocean general circulation model, but it is not known how the accuracy degrades with reduced resolution. Moreover, Gerkema & Shrira (2005) have proposed that the so-called traditional approximation, in which the Coriolis force due to the locally horizontal component of Earth's angular velocity is neglected, is invalid when $\sigma \approx f$ and use a modified β-plane with various predicted consequences at the inertial latitude that have not been well tested.

5. OCEANIC KINETIC ENERGY: TURBULENT CASCADES

The ocean is forced at the surface by momentum, heat, and freshwater fluxes on a wide range of temporal and spatial scales, whereas energy dissipation occurs at molecular scales in short and sudden bursts. To achieve a steady state, energy must be transferred from the forcing to the dissipation scales. **Figures 1** and **2** and **Supplemental Figure 2** show that energy is indeed redistributed across all spatial and temporal scales. The energy transfer is achieved through nonlinear turbulent interactions among oceanic motions at different length scales (recall again the paucity of wave-number spectra). Energy is moved not simply from large to small scales, but also from locations where forcing acts (mostly at the sea surface) to regions in which dissipation is most intense (the surface and bottom boundary layers and coastal areas). The oceanic energy spectrum therefore results from turbulent energy transfers among different regions and different spectral bands. Nonlinear transfers within the subinertial and superinertial frequency bands are effective, whereas transfers between them are apparently weak (e.g., Ford et al. 2000).

5.1. Internal Gravity Waves

Nonlinear interactions in the internal wave band play an important role in the ocean circulation because they transfer energy from large to small scales and provide a link between climatological

forcing and small-scale dissipation. Internal waves are generated mostly as large-scale waves and radiate into the global oceans. As they propagate in physical space, nonlinear wave-wave interactions and other scattering processes cascade their energy through wave-number space to small scales at which they break and dissipate.

The hydrodynamic equations that describe all fluid motions contain advective nonlinearities that produce energy exchange among waves of different frequencies and wave numbers. In strongly turbulent flows, energy is continually exchanged among different scales of motions through "strong, promiscuous interactions" (Phillips 1966) that affect all wave numbers and all frequencies. For internal waves, the interactions are through weak resonant triads of waves.

Internal waves can be described as a stochastic field undergoing resonant triad interactions and are sometimes referred to as wave turbulence (Zakharov et al. 1992). Theoretical studies have been made to examine the way in which internal waves interact with each other in the hope of investigating the apparently stable and universal form of the oceanic internal wave continuum spectrum: Müller et al. (1986) reviewed the early literature, Caillol & Zeitlin (2000) and Lvov & Tabak (2001) provided a new perspective, and Y.V. Lvov, K.L. Polzin & N. Yokoyama (submitted manuscript) showed that all approaches are equivalent. Idealized distortions from the GM spectrum relax rapidly to its universal form, and the equilibrium spectrum displays a steady energy cascade from large to small vertical scales, at which energy is dissipated through a process of wave breaking. The cascade is driven by energy transfer among waves undergoing resonant interactions (McComas & Bretherton 1977). The interactions are efficient at transferring energy to frequencies close to f and to smaller vertical scales at which they can break.

Numerical simulations of energy transfer by interactions within the internal wave field show a net flux toward small vertical scales that increases the shear variance ($|\partial \mathbf{u}/\partial z|^2$) until it overcomes the stratification and the waves break. When the wave field is statistically steady, the rate at which wave breaking dissipates energy approximately equals the rate at which the energy is transferred from large to small scales. Gregg (1989) used this equivalence to derive a semiempirical relation in which the dissipation rate caused by internal waves ε_{INT} is expressed in terms of parameters in the empirical GM model of the internal wave spectrum,

$$\varepsilon_{INT} = 7 \times 10^{-10} \left\langle \frac{N^2}{N_0^2} \right\rangle \left\langle \frac{S_{10}^4}{S_{GM}^4} \right\rangle \mathrm{W\,kg^{-1}}, \tag{10}$$

where $N_0 = 5.2 \times 10^{-3}\ \mathrm{s}^{-1}$ is a reference buoyancy frequency, S_{10} is the observed shear variance at scales greater than 10 m, and S_{GM} is the corresponding variance in the GM spectrum. Are internal waves a primary pathway to energy dissipation in the global ocean? Equation 10 and its subsequent modifications (Gregg et al. 2003) match the observed dissipation rates away from ocean boundaries within a factor of two, and this link strongly suggests that internal waves are such a major pathway.

5.2. Geostrophic Motions

The oceanic KE at subinertial frequencies in mid- and high latitudes is dominated by geostrophic eddies on scales of 50 to 100 km. The dominance of EKE at the oceanic mesoscale was first documented in the early 1970s from ship-going and mooring observations in the Western North Atlantic (e.g., Hua et al. 1986, MODE Group 1978). However, a full characterization of the properties and distribution of the mesoscale eddy field has only been possible in the past 20 years when satellite altimeters provided the first global pictures of the geostrophic circulation at the ocean surface. Three main features emerge from altimetric maps such as the one shown in **Figure 4**: (*a*) Mean flows are strongly inhomogeneous; most of the mean KE is concentrated in narrow

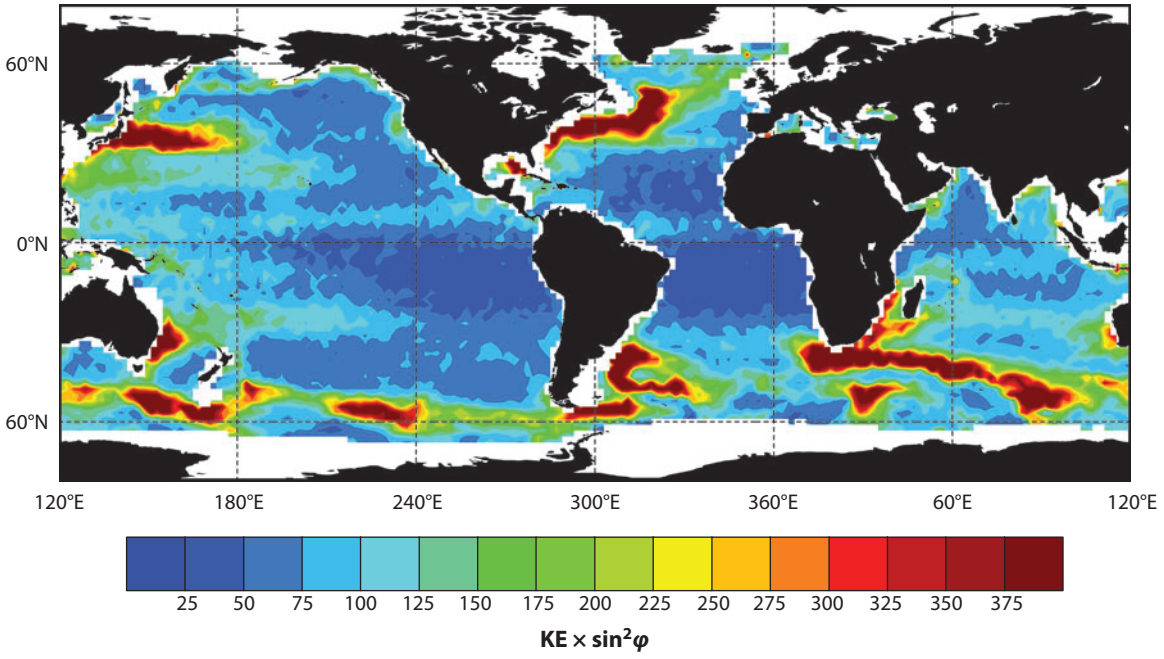

Figure 4

Estimate of the geostrophic kinetic energy (KE) $(\text{cm s}^{-1})^2$ of oceanic variability at the sea surface, here multiplied by $\sin^2 \phi$, where ϕ is the latitude, to avoid the equatorial singularity in noisy data. Note the very large spatial changes of kinetic energy. Figure taken from Wunsch & Stammer 1998.

intense currents such as the Gulf Stream along the Eastern U.S. coast or the Agulhas Current down the east coast of Africa. (*b*) Surface EKE is spatially inhomogeneous, decreasing by an order of magnitude as one moves from the swift mean currents into the interior of the ocean basins. (*c*) The ratio of surface eddy to time mean geostrophic KE is large everywhere, often by a factor of 100 or more, the exception being the Southern Ocean at which it is only a factor of 10 larger.

Conversely, in the tropical oceans, EKE is dominated by seasonal oscillations of the equatorial currents in response to shifts in the intertropical convergence zone and its associated wind patterns. At smaller scales, subinertial variability is associated with tropical instability waves with wavelengths of $O(1000)$ km propagating zonally along the mean equatorial currents.

The coincidence of vigorous EKE and strong currents suggests that the geostrophic eddy field arises from instabilities of more directly forced, persistent large-scale currents. Gill et al. (1974) computed the stability of density and velocity profiles and concluded that baroclinic instability is the dominant generator of the large-scale ocean currents in mid- and high latitudes. These instabilities occur in rotating, stratified fluids with strong currents in thermal wind balance having steeply sloping density surfaces. The energy of the growing perturbations is extracted from the PE stored in the density fronts. Eddies pinch off from the fronts—resulting in flattening of the density surfaces and a release of PE.[5] PE associated with strong ocean currents is approximately 1000 times larger than the KE of the gyre-scale circulation.

[5]Another type of instability, known as barotropic instability, dominates in the tropics. This instability occurs in the presence of strong horizontal shear and derives its energy from the KE of the mean currents.

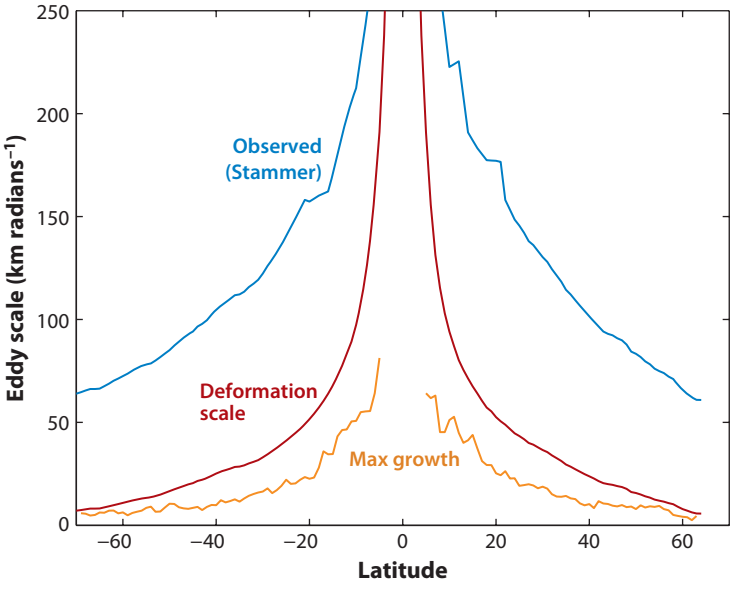

Figure 5

Zonally averaged scales (in kilometers) of the maximum growth rate of baroclinic instability of the main thermocline estimated from hydrography (Smith 2007), the spectral peak of eddy kinetic energy from the analysis of satellite observations by Stammer (1997), and the first deformation radius estimated from Levitus climatology (Chelton et al. 1998). The estimate of the spectral peak of eddy kinetic energy is uncertain. First the altimetric signal is dominated by noise at scales below 100–50 km, and the spectral energy is largest at the smallest wave numbers. Hence the spectral peak estimate is not independent of the choice of filter. Second, the spectral peak is evident only in a small fraction of satellite tracks that cross well-defined coherent eddy structures: The spectral peak does not characterize the background eddy–kinetic energy spectrum, which is close to white.

A distinguishing feature of a baroclinically unstable flow is its intrinsic length scale, known as the Rossby deformation radius,

$$R_d \equiv \sqrt{\frac{g}{f^2 \rho} \Delta\rho \, D},$$

where $\Delta\rho$ is the density change over the distance D, and R_d is the distance a disturbance of that vertical scale propagates in the ocean before reaching geostrophic balance. If D is the depth of the ocean, then among all unstable baroclinic modes, the ones with the largest growth rate have a scale proportional to, but somewhat smaller than, R_d. **Figure 5** shows the zonally averaged Rossby deformation radius in the ocean as a function of latitude from Chelton et al. (1998). (The literature is vague concerning the definition of scale—e.g., whether it is R_d or $R_d/2\pi$—and in some cases, we are unable to determine whether published results are inconsistent because of this fundamental ambiguity.) The decrease of R_d with latitude mostly results from the increase of f with latitude.

Smith (2007) recently examined the linear stability implied by Gouretski & Koltermann's (2004) hydrographic climatology and confirmed that the ocean is baroclinically unstable everywhere. In his model, the fastest growth occurred in regions in which EKE is largest, and quiet regions with reduced KE were only weakly unstable. Smith's maps of eddy growth rates have patterns remarkably similar to those in **Figure 4**. The horizontal scale at which the instabilities develop is proportional to, but somewhat smaller than, R_d (see **Figure 5**). Direct observations are consistent

with the predictions of linear stability analysis; Scott & Wang (2005) find a source of KE at scales close to R_d from a spectral analysis of altimetric observations and interpret it as the conversion of large-scale PE into EKE by baroclinic instability.

We can attempt to estimate the total energy released though baroclinic instability of major currents. Because the source of eddy energy is through the conversion of large-scale PE and is associated with a spindown of the large-scale ocean circulation, one can express the baroclinic release of PE, given by the $g\rho'_{\theta g} w'_g$ term in Equation 5, as an effective eddy stress $\boldsymbol{\tau}_e$ acting against the large-scale ocean circulation,

$$\iint g\overline{\rho'_{\theta g} w'_g}\,\mathrm{d}V = -\iint \frac{\partial \boldsymbol{\tau}_e}{\partial z}\cdot \bar{\boldsymbol{u}}\,\mathrm{d}V, \tag{11}$$

where the overbar denotes a long-term average. Ferreira et al. (2005) estimated $\boldsymbol{\tau}_e$ and the mean circulation with a numerical model of the global ocean constrained with Levitus climatology, leading in Equation 11 to a baroclinic release of 0.3 TW (D. Ferreira, private communication), in the range (0.2–0.8 TW) obtained by Wunsch & Ferrari (2004). [The total is the residual of a 0.5-TW positive release of PE in the upper ocean and a negative value (the creation of PE) below the thermocline.] In summary, baroclinic instability seems capable of releasing 30%–100% of the wind power input to the large-scale circulation.

The approximate agreement between linear theory and observations supports the view that baroclinic instability of mean currents is the main energy source in the geostrophic eddy field. Ocean eddies, however, are observed to be two to ten times larger than the scale of the most unstable waves (**Figure 5**), and their vertical structure is not as surface intensified as predicted by linear stability analysis (Smith 2007), but the ambiguity of scale is on the order of 2π. The observed eddy length scales likely result from nonlinear turbulent interactions that redistribute energy across spatial scales and maintain an equilibrium between the generation and dissipation of geostrophic eddies. Details of these interactions are not fully understood, but a first-order description of oceanic turbulence is emerging owing to the growing number of observations.

In the eddy band, rotation and stratification strongly suppress vertical velocities, and motions are constrained to be quasi-2D. Eddy-eddy interactions in 2D flows result in an inverse cascade of energy to progressively larger-scale motions (Salmon 1998) in contrast to the 3D direct cascade to smaller scales. An inverse cascade of energy in the geostrophic eddy band might therefore be expected. Oceanic flows, however, are quasi-2D in the sense that the horizontal velocity dominates the vertical velocity, but the horizontal velocity varies with depth in contrast to its behavior in purely 2D flows. The direction of the energy cascade is sensitive to these vertical variations.

The vertical structure of the ocean velocity at the mesoscale is well described by an orthogonal set of basis functions given by the eigenfunctions of a Sturm-Liouville problem involving the water depth, the vertically dependent buoyancy frequency, and the Coriolis parameter (e.g., see Vallis 2006). The resulting eigenfunctions are called the baroclinic modes: The m-th mode, ϕ_m, has m zero crossings in the vertical direction. When $m = 0$, the mode is barotropic and represents the depth average, $\phi_0 =$ constant. The eigenvalues λ_m are the inverse of the deformation radii (length^{-1}) of the corresponding modes. The Rossby deformation radius, R_d, is a good approximation to λ_1^{-1}. Theories of geostrophic turbulence (Haidvogel & Held 1980; Rhines 1977; Salmon 1978, 1980; Smith & Vallis 2002) show a direct (downscale) energy cascade for the total baroclinic energy, kinetic and potential, at scales larger than the corresponding deformation radius and an inverse (i.e., upscale) cascade of energy for the barotropic KE (the barotropic mode has almost no PE). A schematic of these energy pathways is shown in **Figure 6**.

Geostrophic turbulence theory predicts that when baroclinic energy in vertical mode m reaches its corresponding deformation radius λ_m, energy is transferred to lower baroclinic modes and

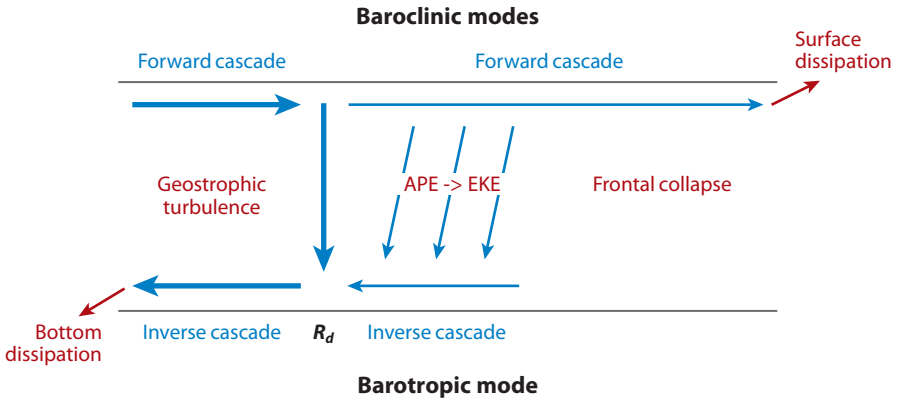

Figure 6

Schematic of the energy pathways in geostrophic turbulence. The horizontal axis represents the horizontal wave number, and the vertical variation is decomposed into the barotropic mode (*lower line*) and the sum of all baroclinic modes (*upper line*). Large-scale forcing maintains the available potential energy (APE), therefore providing energy to the baroclinic mode at very large scales. At these large scales, baroclinic energy is transferred to smaller horizontal scales. At horizontal scales comparable to the Rossby deformation radius, energy is transferred to the barotropic mode and then to larger barotropic scales. Some fraction of the baroclinic energy leaks to smaller scales through surface-intensified baroclinic modes. EKE, eddy kinetic energy.

eventually to the barotropic one (Charney 1971). For a fluid with strong surface-intensified stratification (such as the ocean), the baroclinic modes interact inefficiently with the barotropic mode, and thus energy from higher baroclinic modes collects in the first mode and converges toward the first deformation radius before it finally barotropizes (Flierl 1978, Fu & Flierl 1980, Smith & Vallis 2001). The inverse cascade is the final stage whereby energy in the barotropic mode near the deformation scale moves toward even larger scales. Scott & Arbic (2007) recently showed that the inverse cascade is not confined to the barotropic mode—in numerical simulations, KE associated with the first baroclinic mode also fluxes upscale. In summary, the KE in the mesoscale field moves upscale in deep barotropic and first baroclinic eddies. Numerical simulations suggest that the ratio of energy in the two modes is quite sensitive to the strength of bottom dissipation (Arbic et al. 2007). This paradigm does not apply at the ocean surface, at which energy appears to cascade downscale in surface-trapped modes (Klein et al. 2008).

The presence of a vertical shear due to the large-scale geostrophic currents supports surface-trapped modes in addition to free interior modes. These surface modes tend to extract energy from the interior ones and transfer energy to small horizontal scales at which they become unstable to 3D instabilities and dissipate their energy (Capet et al. 2008a,b; Klein et al. 2008). It is unknown whether the surface modes transfer a substantial amount of KE out of the interior geostrophic eddy field.

Observations broadly support the geostrophic turbulence scenario. Analysis of velocity measurements from mooring data confirms that most of the subinertial EKE resides in equal parts in the barotropic and first baroclinic modes with very little residual in higher ones (Wunsch 1997). Sea-surface height measurements reveal a source of EKE at scales near or larger than the first deformation radius (Scott & Wang 2005). Most of this energy source is likely associated with the development of baroclinic eddies at the expense of the large-scale currents, but some fraction could arise from the nonlinear conversion of energy from high baroclinic modes into the first mode. Scott & Wang (2005) estimated the direction of the energy fluxes from a spectral analysis

of sea-surface data. At scales larger than R_d, KE appears to flow upscale, consistent with the inverse cascade paradigm. The result is a bit ambiguous because the altimeter slope signal reflects only surface velocities, which are dominated by low baroclinic modes with little barotropic contribution, and therefore provide no information on the barotropic energy flux. However, an inverse cascade is also visible in sea-surface height pictures: Mesoscale eddies tend to progressively increase in size downstream of their formation region (Kobashi & Kawamura 2002, Stewart et al. 1996). An increase in eddy size is consistent with the shift from the scale at which they are generated to the larger one at which they equilibrate (**Figure 5**). Altimetric power-law results, however, are fragile: Stammer (1997) and R.B. Scott & D.P. Chambers (submitted manuscript) had to make strong assumptions about the noise contributions to wavelengths shorter than 100–200 km.

Additional support for the geostrophic turbulence paradigm has come from observational (Maximenko et al. 2005) and computational (Nakano & Hasumi 2005, Qiu et al. 2008) evidence of multiple alternating zonal jets primarily, but not solely, in the abyssal ocean, although Huang et al. (2007) showed the real difficulties of obtaining a clear interpretation of data. Zonal jets are believed to result from an interplay between the inverse energy cascade in the barotropic mode and the planetary potential vorticity gradient β (Rhines 1975, Vallis 2006). The hypothesis is that the inverse cascade is nearly arrested meridionally by angular momentum constraints but proceeds in the zonal direction, resulting in oblongated eddies and eventually in alternating jets. Jets are visible in the atmosphere of giants planets in which there is a large gap among the first deformation radius, the scale at which eddies are generated, and the Rhines scale (i.e., the scale at which angular momentum constraints apply). Similar gaps exist in the oceans worldwide, but not in the atmosphere in which the first deformation radius is of $O(1000)$ km and the inverse cascade can span a limited wave-number range (Boer & Shephard 1983, Schneider & Walker 2006).

A serious limitation of the geostrophic turbulence paradigm is that it ignores interactions with bottom topography. The ocean has topography at all scales, particularly in the vicinity of mid-ocean ridges and fracture zones. This structure provides a potential route to shortcut the cascade because energy can be exchanged among different scales via the coupling of different vertical modes in the presence of topography. The presence of an inverse energy cascade and alternating zonal jets at mid-latitudes seems to be good evidence for the plausibility of ignoring (at least to first order) topographic interactions at those latitudes. However, zonal jets are conspicuously absent from the Southern Ocean—the region in which the mean flow is most clearly influenced by topography. This suggests that at high latitudes the interaction with topography is ubiquitous and the idea of a cascade defined in terms of a horizontal wave-number spectrum is incomplete. One expects stronger topographic response at high latitudes because of the weaker overall stratification, the strong atmospheric synoptic forcing, and (in the Southern Ocean) the need to dissipate the very large input of KE and to balance the corresponding momentum injection.

Müller & Frankignoul (1981) and Frankignoul & Müller (1979) pointed out that, in addition to arising from free instabilities of mean currents, geostrophic eddies can be generated by rapidly fluctuating winds. Stammer & Wunsch (1999) found that significant correlations between observed variations in EKE and wind stress are confined to the high latitudes in the North Atlantic and North Pacific, and even there, only a small fraction of the eddy energy could be attributed to direct wind generation. It does appear, however, that the very strong, large-scale, barotropic fluctuations seen in high-latitude altimetric records (e.g., Fukumori et al. 1998, Stammer et al. 2000) are not properly accounted for (the associated KE is small, but their bottom interactions may be very strong). S. Elipot & S. Gille (submitted manuscript) found that rotary spectra of surface winds and upper ocean velocities at subinertial frequencies are predominantly anticyclonic and interpreted this asymmetry as evidence of wind generation of surface eddies because upper-ocean velocities respond preferentially to anticyclonic rotating winds. Whether these surface eddies, with scales

of $O(10)$ km, are dynamically coupled to the larger and more energetic geostrophic eddies that populate the ocean interior is unknown.

5.3. Dissipation of Geostrophic Motions: The End of the Cascade

In summary, large-scale wind and surface fluxes maintain the large-scale reservoir of PE. Baroclinic instability and nonlinear interactions transfer energy to the first baroclinic mode and from there to the barotropic mode, in which an inverse cascade of barotropic KE to larger horizontal scales occurs (Charney 1971, Salmon 1998, Scott & Arbic 2007). Without a dissipation mechanism, the inverse cascade would result in unseen barotropic eddies the size of the ocean basins (**Figure 5**). Some process must drain energy from geostrophic eddy motions and arrest the cascade.

In Wunsch & Ferrari's (2004) energy diagram, the largest uncertainty was associated with the essentially unknown dissipation of the energy contained in the eddy field, which contains over 90% of the KE of the flow (but a minute fraction of the PE). A few candidates exist: (*a*) bottom drag, (*b*) loss of balance (e.g., Molemaker et al. 2005, Williams et al. 2008; see Marshall & Naveira Garabato 2008 for a list of earlier references), (*c*) interactions with the internal wave field, (*d*) continental margin scattering/absorption, and (*e*) suppression by wind work. Other possibilities (e.g., lateral dissipative stresses and damping of eddy motions through air-sea buoyancy fluxes) appear unimportant.

A dissipative interaction with bottom topography can arrest the cascade. As mentioned above, both observations and theory suggest strong spatially variable bottom friction as the main sink. Arbic & Flierl (2004) found that moderate bottom friction is required for the modeled geostrophic turbulence to reproduce the observed amplitudes, vertical structure, and horizontal scales of mid-latitude eddies. Fu et al. (1982), using current meter records, and Gille et al. (2000), globally from altimeter data, inferred that the geostrophic eddy band is suppressed over rough topography—an effect seen in theory for eddies subject to strong bottom friction (Arbic & Flierl 2004, Treguier & Hua 1988).

Wunsch & Ferrari (2004) argued that drag in bottom boundary layers appeared to be too weak to represent the dominant eddy energy sink. From observations, Sen et al. (2008) inferred that between 0.2 and 0.8 TW are dissipated by quadratic bottom boundary layer drag. The uncertainty in the estimate is very large because the dissipation depends on the cube of the bottom geostrophic velocity and is dominated by poorly sampled eddies with exceptionally large velocities. Their upper bound is close to the total estimated power input to the geostrophic field. The lower bound is equal to the estimate reported by Wunsch & Ferrari (2004) and would account for approximately 25% of the total power input into the eddies.

An additional mechanism for damping geostrophic motions is through the generation and radiation of gravity waves from small-scale topographic roughness. Geostrophic flows can radiate waves by flowing over topographic features with scales between u/f and u/N, where u is the magnitude of the geostrophic flow normal to the topographic relief. (Topographic scales outside this range generate evanescent waves.) For typical ocean parameters, the relevant scales lie between 100 m and 10 km. Numerical experiments show that these short topographic waves tend to break within 1 km of the ocean bottom and dissipate their energy locally (Chapman & Haidvogel 1993; M. Nikurashin & R. Ferrari, submitted manuscript). The radiation and breaking of internal gravity waves are reported in observations from two regions of the Southern Ocean characterized by rough topography and energetic barotropic eddies (Naveira Garabato et al. 2004, Polzin & Firing 1997). Marshall & Naveira Garabato (2008) computed an upper bound on the mixing rates induced by topographic wave generation and breaking in the Southern Ocean of $\kappa \leq 5 \times 10^{-3}$ m s^{-1} (a large number). If one uses Wunsch & Ferrari's (2004) equation 8, assigns an area of the Southern Ocean

of 0.6×10^{14} m^2, and assumes this mixing takes place over the bottom 1000 m, in a region in which $N \approx 2\pi/1$/hr, one finds an upper bound of approximately 1 TW for the energy loss by the mesoscale in the Southern Ocean alone (the crudity of this estimate is obvious), already somewhat larger than the estimate of the eddy-production rate from Equation 11.

Molemaker et al. (2007) analyzed high-resolution numerical simulations of an idealized ocean current and found that a loss of geostrophic balance can occur in the ocean, but mostly at the upper-ocean boundary as result of frontogenesis (Hoskins & Bretherton 1972). Surface frontogenesis describes the formation of sharp density gradients as a result of eddy stirring at the ocean boundaries. These fronts have characteristic horizontal scales of a few kilometers, much smaller than mesoscale eddies, so loss of balance can take place. From the perspective of geostrophic turbulence theory, surface frontogenesis represents a direct cascade of baroclinic energy to scales smaller than the deformation radius. A cascade is possible only at the surface because the surface modes at small scales do not interact efficiently with the interior modes and do not barotropize. Observations show that KE is surface intensified at scales smaller than the first deformation radius (Ferrari & Rudnick 2000, LaCasce & Mahadevan 2006) and support the notion that the ocean surface is a primary location for energy transfer to small scales and hence dissipation. Molemaker et al. (2007) found that in idealized ocean simulations of geostrophic turbulence, two-thirds of the eddy energy was fluxed upscale into the barotropic mode and one-third cascaded to smaller scales through surface frontogenesis. Surface dynamics plausibly have an important role in the dissipation of geostrophic EKE.

Other ways exist, beyond spontaneous loss of balance, by which geostrophic energy can be lost to superinertial motions. Müller (1976), and more recently Bühler & McIntyre (2005), showed that the deformations of internal wave packets propagating through the strain due to eddies result in an irreversible extraction of energy from the geostrophic field. Characterization of the energy exchange as a viscous damping of the mesoscale field gives a horizontal viscosity of $\nu_b = 50$ m s^{-1} and a vertical viscosity of $\nu_v = 2.5 \times 10^{-3}$ m s^{-1} (Polzin 2008). Watson (1985) estimated similar viscosities as representative of the energy exchange between mesoscale motions and near-inertial frequency waves through a form of triad interaction. His result showed that Bühler & McIntyre's (2005) inferences apply also in situations in which there is no scale separation between the mesoscale and the internal wave field. From an analysis of altimetric data, Scott & Wang (2005) have reported evidence of energy loss from geostrophic motions at horizontal scales of $O(30)$ km, characteristic of the internal wave field. Because of questions about the data, it is premature to conclude that the observed energy loss is associated with coupling between geostrophic eddies and internal waves, but the possibility is tantalizing.

One can attempt to estimate the eddy energy loss to internal waves based on the horizontal and vertical viscosity coefficients (ν_b and ν_v, respectively) proposed by Watson (1985) and Polzin (2008),

$$\varepsilon \approx \iint \left[\nu_b \left(\frac{\partial \mathbf{u}}{\partial x} \right) \cdot \left(\frac{\partial \mathbf{u}}{\partial x} \right) + \nu_b \left(\frac{\partial \mathbf{u}}{\partial y} \right) \cdot \left(\frac{\partial \mathbf{u}}{\partial y} \right) + \nu_v \left(\frac{\partial \mathbf{u}}{\partial z} \right) \cdot \left(\frac{\partial \mathbf{u}}{\partial z} \right) \right] \mathrm{d}V. \qquad (12)$$

Altimetric velocities reflect mostly the first baroclinic mode (Wunsch 1997), and in most of the ocean, that mode has a characteristic vertical scale $H = 1000$ m and a horizontal scale proportional to the Rossby deformation radius R_d. Typical vertical and horizontal velocity gradients squared are then $(u^2 + v^2)/2H$ and $(u^2 + v^2)/2R_d$, respectively. Altimetric data (Le Traon et al. 1998) provide velocities, and Chelton et al. (1998) computed maps of R_d from hydrography. Assuming that the gradients are confined to the upper 1000 m, the net conversion is approximately 0.35 TW. Although the uncertainty is large, the energy exchange with the background internal wave field remains a potentially important sink of eddy energy. This estimate, however, does conflict

with two properties of the observed internal wave field: (*a*) The energy flux into the background internal wave field, as predicted by the GM spectrum, is an order of magnitude smaller than 0.35 TW. (*b*) The energy content in the internal wave field is believed to be fairly uniform in the ocean interior and depends only on latitude and stratification, whereas the scenario suggests an unobserved strong modulation by the geostrophic eddy field. This story remains unfinished.

Finally, the effects of eddy-like motions on the wind stress act to spin down geostrophic eddies as described in Section 4. The energy diagram in **Supplemental Figure 1** proposes that approximately 13×10^{18} J (13 EJ) are contained in the geostrophic eddy field and that the generation rate by instability mechanisms is such that all the energy could be renewed every 6 months [Thorpe (2005) estimated a 1-year renewal time]. Here it is roughly estimated that 2.6 EJ are KE, the majority being PE. If we suppose that, from the existing fragmentary literature, 10% of the estimated rate of wind work on the ocean goes to spinning down the geostrophic eddy field and take that rate as again roughly 1 TW, then 0.1 TW is available for the stated purpose, and the time to spin down would be 13×10^{18} J/10^{11} $W = 1 \times 10^{8}$ s, or approximately 3 years. Given the crudity of all the numbers, it appears that the mechanism is important. Calculations by Niiler (1969) and Dewar & Flierl (1987), which account for the distortion of Ekman pumping by the vorticity of the ambient motions, appear to be relevant, but no quantitative result exists for the global problem. We have gone from the situation described in Wunsch & Ferrari (2004) of being unable to account for the dissipation of geostrophic turbulence to the opposite case—there are now too many candidates.

6. DISCUSSION

At subinertial frequencies, the ocean circulation is dominated by large-scale currents and geostrophic eddies. The currents are driven by atmospheric winds, whereas the eddy field results from instabilities of the mean currents. Geostrophic eddies account for approximately 90% of the total KE of the oceans, whereas the large-scale circulation is the largest reservoir of PE. EKE acts as a stirrer of tracers and momentum along density surfaces: Geostrophic motions have less shear than internal waves and do not generate overturns and mixing across density surfaces. This eddy stirring is a key element of the meridional overturning circulation of the ocean. For example, the heat budget of the Southern Ocean is dominated by eddies that stir and mix heat poleward against the equatorward heat transport by the wind-driven circulation (Speer et al. 2000).

At equilibrium, the energy flux into the geostrophic eddy field must be balanced by dissipation. It is an open and important question whether some of the dissipation is associated with mixing in the ocean interior. The problem is not well understood because it requires a complete description of the energy pathways from the 100-km scale at which eddies are generated down to the molecular scales, at which irreversible energy dissipation occurs. Theory and altimetric observations suggest that once eddies are generated, eddy-eddy interactions transfer energy primarily to large-scale barotropic and first-baroclinic motions and to small-scale, surface-trapped eddies. If the barotropic and surface eddies are completely dissipated in the bottom and surface turbulent boundary layers, then geostrophic energy does not affect mixing in the ocean interior. However, there is evidence that vigorous internal waves are radiated by barotropic eddies impinging over topography. These waves supposedly radiate and break, resulting in irreversible mixing in the ocean interior. We are not yet in a position to determine whether eddy-driven generation of waves supports a large fraction of the observed abyssal mixing.

KE in the oceanic internal wave band is dominated by inertial waves, frequency $\sigma \approx f$, often carrying high shears. Maintenance of this peak is possible through many energy sources, including resonant interactions of all higher-frequency internal waves, coupling to geostrophic eddies, and the direct generation by local winds. The last mechanism, although known to be effective, in linear

theory tends to produce low vertical wave numbers and hence little shear. Even less is known about how this nearly universal inertial peak is dissipated, and thus it is unclear whether it is a major element in mixing the oceanic abyss, particularly as interactions with topographic features near the critical value are unexplored. Mixing by the internal tide possibly has been overemphasized, but further study is needed.

A major obstacle to progress remains with the difficulty of obtaining direct estimates of frequency and wave-number spectra in the ocean. Each is separately reasonably well-known, but the overlap of space scales corresponding to radically different timescales, and hence physics, precludes any simple understanding of the origin of the KE, and shear, in the open ocean. Observations on wavelengths of 200 km and shorter are particularly needed. Many processes within the near-surface boundary layers, which are poorly observed, have the potential for more effective coupling of deep and upper oceans than is widely appreciated.

Even such apparently well-established mechanisms as momentum transfer from the atmosphere to the ocean are seen to be both qualitatively and quantitatively obscure. That the oceanic flow is important to the calculation of the stress boundary condition has implications both for the generation and dissipation of KE.

There is no shortage of problems remaining in the much discussed area of ocean mixing. The suggestion from 10 years ago that the oceanic energy budget is uncertain by about a factor of two remains valid. For KE, the comparatively huge reservoir represented by the eddy field still cannot be balanced in terms of inputs and outputs within even larger factors, although negative work by the wind and strong bottom dissipation together probably dominate energy removal.

DISCLOSURE STATEMENT

The authors are not aware of any biases that might be perceived as affecting the objectivity of this review.

ACKNOWLEDGMENTS

Our research is supported in part (C.W.) through the National Ocean Partnership Program and the National Aeronautics and Space Administration and by the National Science Foundation award OCE-0612143 (R.F.). Comments from C. Garrett, B. Arbic, S. Smith, D. Chelton, C. Hughes, L. Thomas, M. Alford, A. Naveira Garabato, and E. D'Asaro on various drafts were very helpful. Owing to space limitations, many additional important results, clarifications, and concepts have been reluctantly omitted.

LITERATURE CITED

Alford MH. 2003. Improved global maps and 54-year history of wind-work on ocean inertial motions. *Geophys. Res. Lett.* 30:1424

Alford MH, Whitmont M. 2007. Seasonal and spatial variability of near-inertial kinetic energy from historical moored velocity records. *J. Phys. Oceanogr.* 37:2022–37

Arbic BK, Flierl GR. 2004. Baroclinically unstable geostrophic turbulence in the limits of strong and weak bottom Ekman friction: application to mid-ocean eddies. *J. Phys. Oceanogr.* 34:2257–73

Arbic B, Flierl GR, Scott RB. 2007. Cascade inequalities for forced-dissipated geostrophic turbulence. *J. Phys. Oceanogr.* 37:1470–87

Balmforth N, Young WR. 1999. Radiative damping of near-inertial oscillations in the mixed layer. *J. Mar. Res.* 57:571–84

Behringer D, Regier L, Stommel H. 1979. Thermal feedback on wind-stress as a contributing cause of the Gulf Stream. *J. Mar. Res.* 37:699–709
Boer GJ, Shephard TG. 1983. Large-scale two-dimensional turbulence in the atmosphere. *J. Atmos. Sci.* 40:164–84
Bühler O, McIntyre ME. 2005. Wave capture and wave-vortex duality. *J. Fluid Mech.* 534:67–95
Caillol P, Zeitlin V. 2000. Kinetic equations and stationary energy spectra of weakly nonlinear internal gravity waves. *Dyn. Atmos. Oceans* 32:81–112
Capet X, McWilliams JC, Molemaker MJ, Shchepetkin AF. 2008a. Mesoscale to submesoscale transition in the California current system. Part I: flow structure, eddy flux, and observational tests. *J. Phys. Oceanogr.* 38:29–43
Capet X, McWilliams JC, Molemaker MJ, Shchepetkin AF. 2008b. Mesoscale to submesoscale transition in the California current system. Part II: frontal processes. *J. Phys. Oceanogr.* 38:44–64
Chandrasekhar S. 1968. *Hydrodynamic and Hydromagnetic Stability*. New York: Oxford Univ. Press. 652 pp.
Chapman DC, Haidvogel DB. 1993. Generation of internal lee waves trapped over a tall isolated seamount. *Astrophys. Fluid Dyn.* 69:33–54
Charney JG. 1971. Geostrophic turbulence. *J. Atmos. Sci.* 28:1087–95
Chelton DB, DeSzoeke RA, Schlax MG, El Naqqar K, Siwertz N. 1998. Geographical variability of the first baroclinic Rossby radius of deformation. *J. Phys. Oceanogr.* 28:433–60
Chelton DB, Schlax MG, Freilich MH, Millif RF. 2004. Satellite measurements reveal persistent small-scale features in ocean winds. *Science* 303:978–83
Cornillon P, Park KA. 2001. Warm core ring velocities inferred from NSCAT. *Geophys. Res. Lett.* 28:575–78
Corrsin S. 1959. Atmospheric diffusion and air pollution. In *Advances in Geophysics*, Vol. 6, ed. F Frenkiel, P Sheppard, pp. 441–48. New York: Academic
Csanady GT. 2001. *Air-Sea Interaction: Laws and Mechanisms*. Cambridge: Cambridge Univ. Press. 248 pp.
D'Asaro EA. 1985. The energy flux from the wind to near-inertial motions in the surface mixed layer. *J. Phys. Oceanogr.* 15:1043–59
D'Asaro EA. 1989. The decay of wind-forced mixed layer inertial oscillations due to the beta effect. *J. Geophys. Res.* 94:2045–56
D'Asaro EA, Lien RC. 2000. Lagrangian measurements of waves and turbulence in stratified flows. *J. Phys. Oceanogr.* 30:641–55
Dawe JT, Thompson L. 2006. Effect of ocean surface currents on wind stress, heat flux and wind power input to the ocean. *Geophys. Res. Lett.* 33:L09604
Defant A. 1961. *Physical Oceanography*. New York: Pergamon
Dewar WK, Flierl GR. 1987. Some effects of the wind on rings. *J. Phys. Oceanogr.* 17:1653–67
Duhaut THA, Straub DN. 2006. Wind stress dependence on ocean surface velocity: implications for mechanical energy input to ocean circulation. *J. Phys. Oceanogr.* 36:202–11
Emanuel K. 2003. A similarity hypothesis for air–sea exchange at extreme wind speeds. *J. Atmos. Sci.* 60:1420–28
Eriksen CC. 1985. Implications of ocean bottom reflection for internal wave spectra and mixing. *J. Phys. Oceanogr.* 15:1145–56
Eriksen CC. 1998. Internal wave reflection and mixing at Fieberling Guyot. *J. Geophys. Res.* 103:2977–94
Ferrari R, Rudnick DL. 2000. Thermohaline structure of the upper ocean. *J. Geophys. Res.* 105:16857–83
Ferreira D, Marshall J, Heimbach P. 2005. Estimating eddy stresses by fitting dynamics to observations using a residual-mean ocean circulation model and its adjoint. *J. Phys. Oceanogr.* 35:1891–910
Flierl GR. 1978. Models of vertical structure and the calibration of two-layer models. *Dyn. Atmos. Oceans* 2:341–81
Ford R, McIntyre ME, Norton WA. 2000. Balance and the slow quasimanifold: some explicit results. *J. Atmos. Sci.* 57:1236–54
Frankignoul C, Müller P. 1979. Quasi-geostrophic response of an infinite beta-plane ocean to stochastic forcing by the atmosphere. *J. Phys. Oceanogr.* 9:104–127
Fu L-L. 1981. Observations and models of inertial waves in the deep ocean. *Revs. Geophys. Space Phys.* 19:141–70
Fu L-L, Flierl GR. 1980. Nonlinear energy and enstrophy transfers in a realistically stratified ocean. *Dyn. Atmos. Oceans* 4:219–46

Fu L-L, Keffer T, Niiler P, Wunsch C. 1982. Observations of mesoscale variability in the western North Atlantic: a comparative study. *J. Mar. Res.* 40:809–48
Fukumori I, Raghunath R, Fu L-L. 1998. Nature of global large-scale sea level variability in relation to atmospheric forcing: a modeling study. *J. Geophys. Res.* 103:5493–512
Gage KS, Nastrom GD. 1986. Spectrum of atmospheric vertical displacements and spectrum of conservative scalar passive additives due to quasi-horizontal atmospheric motions. *J. Geophys. Res.* 91:13211–16
Garrett C. 2001. What is the "near-inertial" band and why is it different from the rest of the internal wave spectrum? *J. Phys. Oceanogr.* 31:962–71
Garrett C, Kunze E. 2007. Internal tide generation in the deep ocean. *Annu. Rev. Fluid Mech.* 39:57–87
Garrett CJR, Munk WH. 1972. Space-time scales of internal waves. *Geophys. Fluid Dyn.* 3:225–64
Gerkema T, Shrira VI. 2005. Near-inertial waves on the "nontraditional" β-plane. *J. Geophys. Res.* 110:C1003
Gill AE. 1984. On the behavior of internal waves in the wakes of storms. *J. Phys. Oceanogr.* 14:1129–51
Gill AE, Green JSA, Simmons AJ. 1974. Energy partition in the large-scale ocean circulation and the production of mid-ocean eddies. *Deep-Sea Res.* 21:499–528
Gille ST. 2005. Statistical characterization of zonal and meridional ocean wind stress. *J. Atmos. Ocean. Technol.* 22:1353–72
Gille ST, Yale MM, Sandwell DT. 2000. Global correlation of mesoscale ocean variability with seafloor roughness from satellite altimetry. *Geophys. Res. Lett.* 27:1251–54
Gouretski VV, Koltermann KP. 2004. WOCE global hydrographic climatology. *Tech. Rep. Ber. Bundesamtes Seeschifffahrt Hydrogr. No. 35/2004*, Hamburg und Rostock
Gregg MC. 1989. Scaling turbulent dissipation in the thermocline. *J. Geophys. Res.* 94:9686–98
Gregg MC, Sanford TB, Winkel DP. 2003. Reduced mixing from the breaking of internal waves in equatorial waters. *Nature* 422:513–15
Haidvogel DB, Held IM. 1980. Homogeneous quasi-geostrophic turbulence driven by a uniform temperature gradient. *J. Atmos. Sci.* 37:2644–60
Hibiya T, Nagasawa M, Niwa Y. 2002. Nonlinear energy transfer within the oceanic internal wave spectrum at mid and high latitudes. *J. Geophys. Res.* 107:3207
Hibiya T, Niwa Y, Nakajima K, Suginohara N. 1996. Direct numerical simulation of the roll-off range of internal wave shear spectra in the ocean. *J. Geophys. Res.* 101:14123–29
Hogg NG. 1987. A least-squares fit of the advective-diffusive equations in Levitus Atlas data. *J. Mar. Res.* 45:347–75
Hoskins BJ, Bretherton FP. 1972. Atmospheric frontogenesis models: mathematical formulation and solution. *J. Atmos. Sci.* 29:11–37
Houghton JT, ed. 2001. *Climate Change 2001: The Scientific Basis*. Cambridge: Cambridge Univ. Press. 881 pp.
Hua BL, McWilliams JC, Klein P. 1998. Lagrangian acceleration and dispersion in geostrophic turbulence. *J. Fluid Mech.* 366:87–108
Hua BL, McWilliams JC, Owens WB. 1986. An objective analysis of the POLYMODE local dynamics experiment II: stream function and potential vorticity. *J. Phys. Oceanogr.* 16:506–22
Huang H-P, Kaplan A, Curchitser EN, Maximenko NA. 2007. The degree of anisotropy for mid-ocean currents from satellite observations and an eddy-permitting model simulation. *J. Geophys. Res.* 112:C09005
Hughes CW, Wilson C. 2008. Wind work on the geostrophic ocean circulation: an observational study of the effect of small scales in the wind stress. *J. Geophys. Res.* 113:C02016
Hughes GO, Griffiths RW. 2006. A simple convective model of the global overturning circulation, including effects of entrainment into sinking regions. *Ocean Model.* 12:46–79
Intergov. Panel Climate Change (IPCC). 2007. *Climate Change 2007: The Physical Science Basis*. Cambridge: Cambridge Univ. Press. 1009 pp.
Ivey GN, Winters KB, de Silva IPD. 2000. Turbulent mixing in a sloping benthic boundary layer energized by internal waves. *J. Fluid Mech.* 418:59–76
Ivey GN, Winters KB, Koseff JR. 2008. Density stratification, turbulence, but how much mixing? *Annu. Rev. Fluid Mech.* 40:169–84
Jones ISF, Toba Y. 2001. *Wind Stress over the Ocean*. Cambridge: Cambridge Univ. Press. 305 pp.

Katz EJ. 1975. Tow spectra from MODE. *J. Geophys. Res.* 80:1163–67
Klein P, Hua BL, Lapeyre G, Capet X, Le Gentil S, Sasaki H. 2008. Upper ocean turbulence from high-3D resolution simulations. *J. Phys. Oceanogr.* In press
Klein P, Lapeyre G, Large WG. 2004. Wind ringing of the ocean in presence of mesoscale eddies. *Geophys. Res. Lett.* 31:L15306
Klymak JM, Moum JN, Nash JD, Kunze E, Girton JB, et al. 2006. An estimate of tidal energy lost to turbulence at the Hawaiian Ridge. *J. Phys. Oceanogr.* 36:1148–64
Kobashi F, Kawamura H. 2002. Seasonal variation and instability nature of the North Pacific Subtropical Countercurrent and the Hawaiian Lee Countercurrent. *J. Geophys. Res.* 107:3185
Kunze E, Sanford TB. 1986. Near-inertial wave interactions with mean flow and bottom topography near Caryn Seamount. *J. Phys. Oceanogr.* 16:109–20
LaCasce JH. 2007. Lagrangian statistics from oceanic and atmospheric observations. In *Transport in Geophysical Flows, Ten Years After*, ed. A Provenzale, JB Weiss, pp. 165–218. Berlin: Springer-Verlag
LaCasce J, Mahadevan A. 2006. Estimating subsurface horizontal and vertical velocities from sea surface temperature. *J. Mar. Res.* 64:695–721
Lai DY, Sanford TB. 1986. Observations of hurricane-generated near-inertial slope modes. *J. Phys. Oceanogr.* 16:657–66
Large WG, Danabasoglu G. 2006. Attribution and impacts of upper-ocean biases in CCSM3. *J. Clim.* 19:2325–46
Leaman KD. 1976. Observations on the vertical polarization and energy flux of near-inertial waves. *J. Phys. Oceanogr.* 6:894–908
Le Traon PY, Nadal F, Ducet N. 1998. An improved mapping method of multisatellite altimeter data. *J. Atmos. Ocean. Technol.* 15:522–34
Lvov YV, Tabak E. 2001. Hamiltonian formalism and the Garrett-Munk spectrum of internal waves in the ocean. *Phys. Rev. Lett.* 87:168501
MacKinnon JA, Winters KB. 2005. Subtropical catastrophe: significant loss of low-mode tidal energy at 28.9°. *Geophys. Res. Lett.* 32:L15605
Marshall DP, Naveira Garabato AC. 2008. A conjecture on the role of bottom-enhanced diapycnal mixing in the parameterization of geostrophic eddies. *J. Phys. Oceanogr.* 38:1607–13
Maximenko NA, Bang B, Sasaki H. 2005. Observational evidence of alternating zonal jets in the world ocean. *Geophys. Res. Lett.* 32:L12607
McComas CH, Bretherton FP. 1977. Resonant interaction of oceanic internal waves. *J. Geophys. Res.* 82:1397–412
Middleton JF. 1985. Drifter spectra and diffusivities. *J. Mar. Res.* 43:37–55
MODE Group. 1978. The mid-ocean dynamics experiment. *Deep-Sea Res.* 25:859–910
Mohelis J, Llewelyn Smith SG. 2001. Radiation of mixed layer near-inertial oscillations into the ocean interior. *J. Phys. Oceanogr.* 31:1550–60
Molemaker MJ, McWilliams JC, Capet X. 2008. Balanced and unbalanced routes to dissipation in an equilibrated eddy flow. *J. Fluid Mech.* In press
Molemaker MJ, McWilliams JC, Yavneh I. 2005. Baroclinic instability and loss of balance. *J. Phys. Oceanogr.* 35:1505–17
Moum JN. 1996. Energy-containing scales of turbulence in the ocean thermocline. *J. Geophys. Res.* 101:14095–109
Müller P. 1976. Diffusion of momentum and mass by internal gravity waves. *J. Fluid Mech.* 77:789–823
Müller P, Frankignoul C. 1981. Direct atmospheric forcing of geostrophic eddies. *J. Phys. Oceanogr.* 11:287–308
Müller P, Holloway G, Henyey F, Pomphrey N. 1986. Nonlinear interactions among internal gravity waves. *Rev. Geophys.* 24:493–536
Munk W. 1981. Internal waves and small-scale processes. *Evolution of Physical Oceanography: Scientific Surveys in Honor of Henry Stommel*, ed. BA Warren, C Wunsch, pp. 264–91. Cambridge, MA: MIT Press
Munk W, Phillips N. 1968. Coherence and band structure of inertial motion in the sea. *Rev. Geophys.* 6:447–72
Munk W, Wunsch C. 1998. Abyssal recipes II: energetics of tidal and wind mixing. *Deep-Sea Res.* 45:1976–2009

Nakano H, Hasumi H. 2005. A series of zonal jet embedded in the broad zonal flows in the Pacific obtained in eddy-permitting ocean circulation models. *J. Phys. Oceanogr.* 35:474–88
Nash JD, Alford MH, Kunze E, Martini K, Kelly S. 2007. Hotspots of deep ocean mixing on the Oregon continental slope. *Geophys. Res. Lett.* 34:L01605
Naveira Garabato AC, Polzin KL, King BA, Heywood KJ, Visbeck M. 2004. Widespread intense turbulent mixing in the Southern Ocean. *Science* 303:210–33
Niiler PP. 1969. On the Ekman divergence in an oceanic jet. *J. Geophys. Res.* 74:7048–52
Niwa Y, Hibiya T. 1999. Response of the deep ocean internal wave field to traveling midlatitude storms as observed in long-term current measurements. *J. Geophys. Res.* 104:10981–89
Pedlosky J. 1996. *Ocean Circulation Theory*. Berlin: Springer-Verlag. 450 pp.
Phillips HE, Rintoul SR. 2000. Eddy variability and energetics from direct current measurements in the Antarctic Circumpolar Current south of Australia. *J. Phys. Oceanogr.* 30:3050–76
Phillips OM. 1966. *The Dynamics of the Upper Ocean*. New York: Cambridge Univ. Press. 269 pp.
Pinkel R. 2008. Advection, phase distortion, and the frequency spectrum of fine-scale fields in the sea. *J. Phys. Oceanogr.* 38:291–313
Plueddemann AJ, Farrar JT. 2006. Observations and models of the energy flux from the wind to mixed-layer inertial currents. *Deep-Sea Res. II* 53:5–30
Plumb RA, Ferrari R. 2005. Transformed Eulerian-mean theory. Part 1: Nonquasigeostrophic theory for eddies on a zonal-mean flow. *J. Phys. Oceanogr.* 35:165–74
Pollard RT, Millard RC. 1970. Comparison between observed and simulated wind-generated inertial oscillations. *Deep-Sea Res.* 17:813–21
Polzin K. 2008. Mesoscale eddy–internal wave coupling. I. Symmetry, wave capture and results from the Mid-Ocean Dynamics Experiment. *J. Phys. Oceanogr.* In press
Polzin K, Firing E. 1997. Estimates of diapycnal mixing using LADCP and CTD data from I8. *Int. WOCE Newsl.* 29:39–42
Qiu B, Scott RB, Chen S. 2008. Length scales of eddy generation and nonlinear evolution of the seasonally-modulated South Pacific Subtropical Countercurrent. *J. Phys. Oceanogr.* In press
Rainville L, Pinkel R. 2006. Baroclinic energy flux at the Hawaiian Ridge: observations from the R/P FLIP. *J. Phys. Oceanogr.* 36:1104–22
Rhines PB. 1975. Waves and turbulence on a β-plane. *J. Fluid Mech.* 69:417–43
Rhines PB. 1977. The dynamics of unsteady currents. In *The Sea*, Vol. 6: *Marine Modeling*, ed. ED Goldberg, IN McCave, JJ O'Brien, JH Steele, pp. 189–318. New York: Wiley & Sons
Risien CB, Chelton DB. 2008. A global climatology of surface wind and wind stress fields from 8 years of QuikSCAT scatterometer data. *J. Phys. Oceanogr.* In press
Rudnick DL, Boyd TJ, Brainard RE, Carter GS, Egbert GD, et al. 2003. From tides to mixing along the Hawaiian Ridge. *Science* 301:355–57
Salmon R. 1978. Two-layer quasigeostrophic turbulence in a simple special case. *Geophys. Astrophys. Fluid Dyn.* 10:25–52
Salmon R. 1980. Baroclinic instability and geostrophic turbulence. *Geophys. Astrophys. Fluid Dyn.* 15:167–211
Salmon R. 1998. *Lectures on Geophysical Fluid Dynamics*. New York: Oxford Univ. Press. 378 pp.
Schneider T, Walker CC. 2006. Self-organization of atmospheric macroturbulence into critical states of weak nonlinear eddy-eddy interactions. *J. Atmos. Sci.* 63:1569–86
Scott RB, Arbic BK. 2007. Spectral energy fluxes in geostrophic turbulence: implications for ocean energetics. *J. Phys. Oceanogr.* 37:673–88
Scott RG, Wang FM. 2005. Direct evidence of an oceanic inverse kinetic energy cascade from satellite altimetry. *J. Phys. Oceanogr.* 35:1650–66
Sen A, Scott RB, Arbic BK. 2008. Global energy dissipation rate of deep-ocean low-frequency flows by quadratic bottom boundary layer drag: computations from current-meter data. *Geophys. Res. Lett.* 35:L09606
Smith KS. 2007. The geography of linear baroclinic instability in Earth's oceans. *J. Mar. Res.* 29:655–83
Smith KS, Vallis GK. 2001. The scales and equilibration of midocean eddies: freely evolving flow. *J. Phys. Oceanogr.* 31:554–71

Smith KS, Vallis GK. 2002. The scales and equilibration of midocean eddies: forced-dissipative flow. *J. Phys. Oceanogr.* 32:1699–720
Speer K, Rintoul SR, Sloyan B. 2000. The diabatic Deacon cell. *J. Phys. Oceanogr.* 30:3212–22
Stammer D. 1997. On eddy characteristics, eddy mixing and mean flow properties. *J. Phys. Oceanogr.* 28:727–39
Stammer D, Wunsch C. 1999. Temporal changes in the mesoscale variability of the oceans. *Deep-Sea Res. II* 46:77–108
Stammer D, Wunsch C, Ponte R. 2000. De-aliasing global altimetric records with a general circulation model. *Geophys. Res. Lett.* 27:1175–78
Stewart RH, Shum CK, Tapley B, Ji L. 1996. Statistics of geostrophic turbulence in the Southern Ocean from satellite altimetry and numerical models. *Phys. D* 98:599–613
St. Laurent L, Simmons H. 2006. Estimates of power consumed by mixing in the ocean interior. *J. Clim.* 6:4877–90
Stockwell RG, Large WG, Milliff RF. 2004. Resonant inertial oscillations in moored buoy ocean surface winds. *Tellus A* 56:536–47
Taylor GI. 1921. Diffusion by continuous movements. *Proc. Lond. Math. Soc.* 2:196–211
Thorpe SA. 2005. *The Turbulent Ocean*. Cambridge: Cambridge Univ. Press. 439 pp.
Toggweiler JR, Samuels B. 1995. Effect of Drake Passage on the global thermohaline circulation. *Deep-Sea Res.* 42:477–500
Toole JM. 2007. Temporal characteristics of abyssal finescale motions above rough bathymetry. *J. Phys. Oceanogr.* 37:409–27
Treguier AM, Hua BL. 1988. Influence of bottom topography on stratified quasi-geostrophic turbulence in the ocean. *Geophys. Astrophys. Fluid Dyn.* 43:265–305
Vallis GK. 2006. *Atmospheric and Oceanic Fluid Dynamics: Fundamentals and Large-Scale Ciculation*. Cambridge: Cambridge Univ. Press. 745 pp.
van Haren H. 2005. Spatial variability of deep-ocean motions above an abyssal plain. *J. Geophys. Res.* 109:C12014
von Storch JS, Sasaki H, Marotzke J. 2007. Wind-generated power input to the deep ocean: an estimate using a 1/10° general circulation model. *J. Phys. Oceanogr.* 37:657–72
Wang W, Huang RX. 2004. Wind energy input to the surface waves. *J. Phys. Oceanogr.* 34:1276–80
Watson KM. 1985. Interaction between internal waves and mesoscale flows. *J. Phys. Oceanogr.* 15:1296–311
Webb DJ, Suginohara N. 2001. Vertical mixing in the ocean. *Nature* 409:37
Whitehead J, Wang W. 2008. A laboratory model of vertical ocean circulation driven by mixing. *J. Phys. Oceanogr.* 38:1091–106
Williams PD, Haine TWN, Eyink GL, Read PL, Ring D. 2008. Inertia-gravity waves emitted from quasi-balanced flow: origins, properties and consequences. *J. Atmos. Sci.* In press
Wunsch C. 1976. Geographical variability of the internal wave field: a search for sources and sinks. *J. Phys. Oceanogr.* 6:471–85
Wunsch C. 1997. The vertical partition of oceanic horizontal kinetic energy. *J. Phys. Oceanogr.* 27:1770–94
Wunsch C. 1998. The work done by the wind on the oceanic general circulation. *J. Phys. Oceanogr.* 28:2332–40
Wunsch C. 2007. The past and future ocean circulation from a contemporary perspective. In *Ocean Circulation: Mechanisms and Impacts*, ed. A Schmittner, JCH Chiang, SR Hemming, pp. 53–74. Geophys. Monogr. 73. Washington, DC: Am. Geophys. Union
Wunsch C, Ferrari R. 2004. Vertical mixing, energy, and the general circulation of the oceans. *Annu. Rev. Fluid. Mech.* 36:281–314
Wunsch C, Stammer D. 1998. Satellite altimetry, the marine geoid and the oceanic general circulation. *Annu. Rev. Earth Planet. Sci.* 26:219–54
Xing J, Davies AM. 2002. Processes influencing the nonlinear interaction between inertial oscillations, near inertial waves and internal tides. *Geophys. Res. Lett.* 29:1067
Xing J, Davies AM. 2006. Processes influencing tidal mixing in the region of sills. *Geophys. Res. Lett.* 33:L04603
Young WR, Ben Jelloul M. 1997. Propagation of near-inertial oscillations through a geostrophic flow. *J. Mar. Res.* 55:735–66
Zang X, Wunsch C. 2001. Spectral description of low frequency oceanic variability. *J. Phys. Oceanogr.* 31:3073–95

Zakharov VE, L'vov VS, Falkovich G. 1992. *Kolmogorov Spectra of Turbulence*. Berlin: Springer-Verlag
Zervakis V, Levine MD. 1995. Near-inertial energy propagation from the mixed layer: theoretical considerations. *J. Phys. Oceanogr.* 25:2872–89
Zhai X, Greatbatch RJ. 2007. Wind work in a model of the northwest Atlantic Ocean. *Geophys. Res. Lett.* 34:L04606
Zhai X, Greatbatch RJ, Eden C. 2007. Spreading of near-inertial energy in a 1/12° model of the North Atlantic Ocean. *Geophys. Res. Lett.* 34:L10609

Annual Review of
Fluid Mechanics

Volume 41, 2009

Contents

Indexes

Errata

An online log of corrections to *Annual Review of Fluid Mechanics* articles may be found at http://fluid.annualreviews.org/errata.shtml